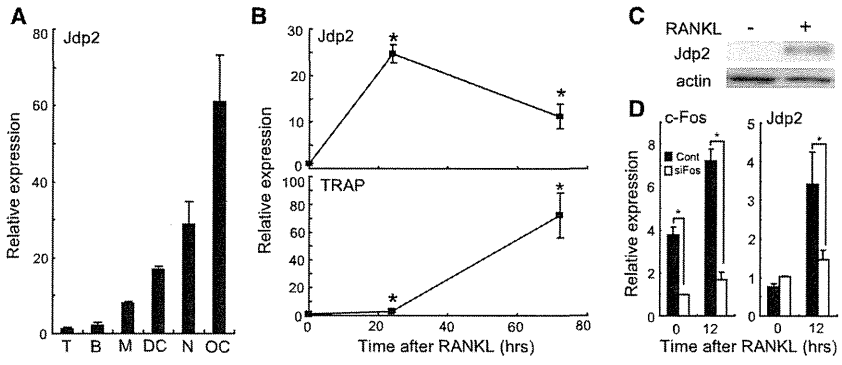

Figure 1. Jdp2 Expression

(A) qPCR analysis of Jdp2 in splenic T cells (T), B cells (B), DCs (DC), neutrophils (N), and primary bone marrow osteoclasts (OC) (n = 3).

(B) qPCR analysis of Jdp2 in MDMs in response to RANKL stimulation. *p < 0.05 versus 0 hr (n = 3).

(C) MDMs were stimulated with 50 ng/ml RANKL for 30 hr. Jdp2 levels were analyzed by protein immunoblotting.

(D) MDMs were transfected with control siRNA (Cont) or c-Fos-specific siRNA (siFos) and stimulated with 50 ng/ml RANKL for 12 hr. c-Fos and Jdp2 levels were measured by qPCR (n = 3).

*p < 0.05 versus control siRNA. Error bars, SE.

development of neutrophils. For example, granulocyte colony-stimulating factor (G-CSF) plays a pivotal role in proliferation of neutrophil precursors via activation of STAT3 (Lieschke et al., 1994). The CCAAT/enhancer binding protein (C/EBP) family is also critically involved in neutrophil differentiation. In particular, C/EBPα is considered a master regulator of neutrophils because C/EBPα-deficient mice lack neutrophils (Zhang et al., 1998). C/EBPε is involved in proper neutrophil differentiation, because neutrophils from C/EBPε-deficient mice have abnormal respiratory burst activity and lack secondary and tertiary granules (Yamanaka et al., 1997). Recent reports have also implicated the transcription factors Gfi-1 (Hock et al., 2003) and Ikaros (Dumortier et al., 2003) in proper differentiation of neutrophils. Overall, these findings suggest that neutrophil differentiation is orchestrated by interplay among several transcription factors.

Despite its importance in in vitro osteoclastogenesis and several implications for its activity in myeloid lineage cells, the roles of Jdp2 in vivo and its pleiotropic functions are completely unknown. Here, we generated *Jdp2*$^{-/-}$ mice and discovered critical roles of Jdp2 not only in bone homeostasis but also in proper differentiation of neutrophils.

RESULTS

Jdp2$^{-/-}$ Mice Are Osteopetrotic because of Impaired Osteoclastogenesis

First, we examined Jdp2 expression in mature myeloid cells, such as macrophages, dendritic cells (DCs), neutrophils, and osteoclasts. Jdp2 expression was substantially higher in these cells than in lymphoid cells, such as T and B cells (Figure 1A). Because Jdp2 expression was highest in osteoclasts (Figure 1A), we focused on the regulation of Jdp2 expression in response to RANKL. Jdp2 expression was significantly increased in M-CSF-derived macrophages (MDMs) after RANKL stimulation (Figures 1B and 1C) but not after LPS stimulation (Figure S1 available online). This transcriptional induction was dependent on c-Fos (based on siRNA knockdown), which is recognized as a pivotal transcription factor for osteoclastogenesis (Figure 1D). The existence of this c-Fos-Jdp2 axis prompted us to explore the role of Jdp2 in RANKL-induced osteoclastogenesis.

To evaluate osteoclastogenesis in vitro, *Jdp2*$^{-/-}$ mice were generated (Figures S2A–S2C). Surprisingly, in vitro RANKL-induced osteoclastogenesis and resorption pit formation were completely abrogated in *Jdp2*$^{-/-}$ cells (Figure 2A). We also evaluated the characteristics of splenic macrophages and found that the populations were similar between wild-type and *Jdp2*$^{-/-}$ cells (Figures S2D, S2E, and S2G). In addition, *Jdp2*$^{-/-}$ MDMs exhibited normal proliferation (Figure S2F) and RANK and c-fms expression (Figure S2H).

As previously reported (Kawaida et al., 2003), induction of osteoclast-associated genes, including TRAP and CTSK, was abrogated in *Jdp2*$^{-/-}$ cells, whereas c-Fos induction was comparable between wild-type and *Jdp2*$^{-/-}$ cells (Figure 2B). We also found that induction of NFATc1 mRNA and DNA binding of NFATc1 to its promoter was partially suppressed in *Jdp2*$^{-/-}$ cells in response to RANKL (Figures S2I and S2J). In addition, Jdp2 had no effect on NFATc1 binding to its promoter region (Figure S2K). Furthermore, DNA binding of NF-κB p65 was normal (Figure S2L). The expression levels of Blimp1, a positive regulator of osteoclastogenesis (Nishikawa et al., 2010), and Blimp1 target genes, such as *Irf8* and *Bcl6*, were comparable (Figure S2M). RANKL-induced calcium oscillation was normal in *Jdp2*$^{-/-}$ cells (Figure S2N). Because TREM2 is required for osteoclast multinucleation (Humphrey et al., 2006), we examined the TREM2 expression levels in wild-type and *Jdp2*$^{-/-}$ MDMs but found no difference (Figure S2O). When TREM2 was stimulated by antibody, wild-type MDMs formed increased numbers of osteoclasts. In contrast, TREM2 stimulation had no effect on osteoclastogenesis of *Jdp2*$^{-/-}$ MDMs (Figures S2P and S2Q). Finally, retrovirus reconstitution of Jdp2 in *Jdp2*$^{-/-}$ MDMs rescued RANKL-induced osteoclastogenesis (Figures S2R and S2S). Together, these results indicate that the c-Fos-Jdp2 axis is critical for controlling osteoclastogenesis via proper induction of NFATc1 and osteoclastogenic genes, such as *TRAP* and *CTSK*.

These findings prompted us to explore the role of Jdp2 in in vivo bone homeostasis. No apparent abnormalities were observed in *Jdp2*$^{-/-}$ mice, although they did exhibit slightly shortened femurs (Figure 2D). Radiographic analysis of the femurs showed that *Jdp2*$^{-/-}$ mice had osteopetrosis accompanied by marked increases in trabecular bone volume and number, compared with wild-type mice (Figures 2C, 2F, and 2G). These findings were further supported by increased bone mineral density (BMD) in the full-length femurs of *Jdp2*$^{-/-}$ mice (Figure 2E). Sections of proximal tibias from *Jdp2*$^{-/-}$ mice also showed increased trabecular bone volume and number (Figures 2H and 2I). Histomorphometric analysis revealed

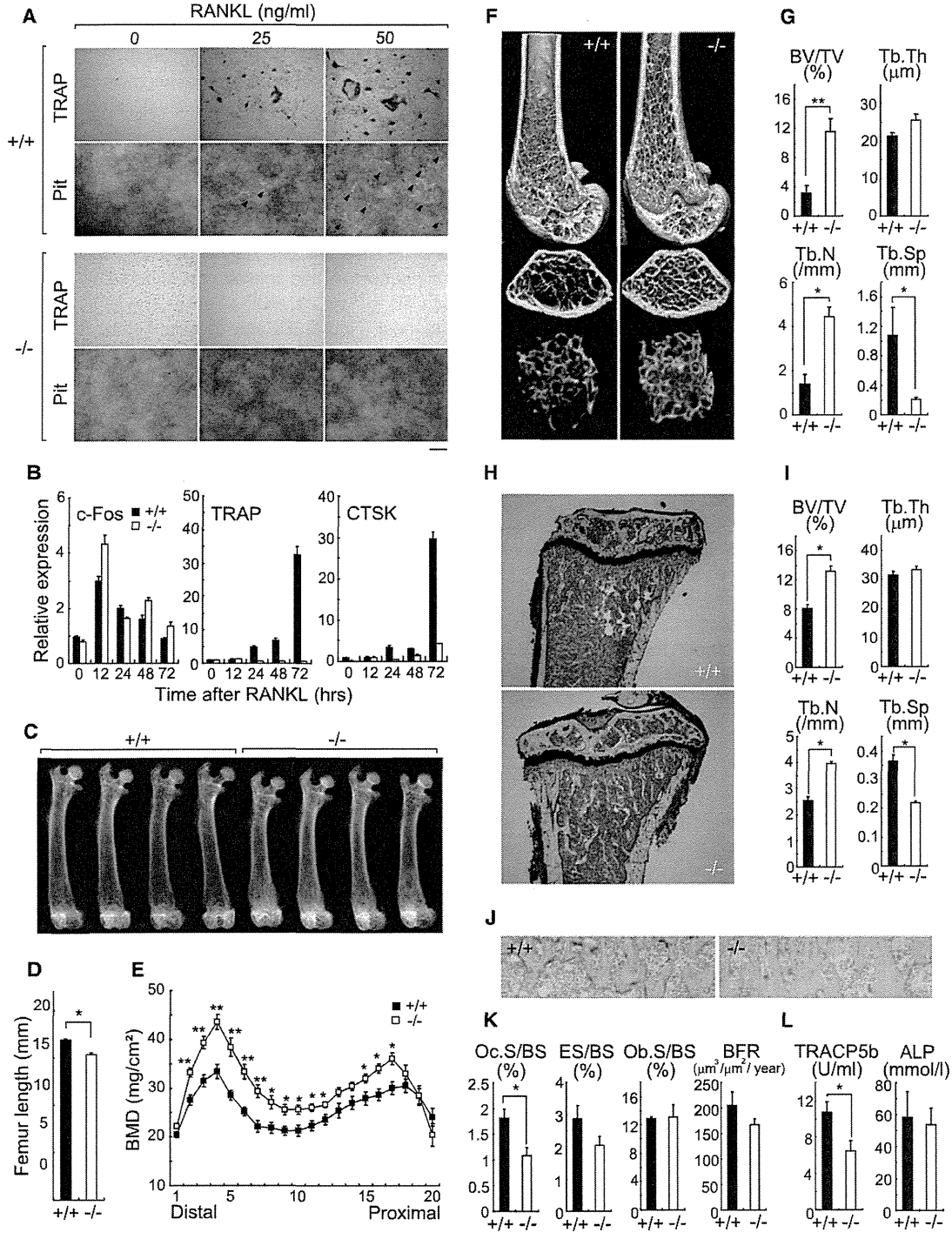

Figure 2. Impaired Osteoclastogenesis in *Jdp2*$^{-/-}$ Mice

(A) MDMs from wild-type and *Jdp2*$^{-/-}$ mice were cultured with the indicated concentrations of RANKL. Representative TRAP staining and resorption pits (arrowheads) are shown. Scale bar represents 200 μm.

(B) qPCR analysis of c-Fos, TRAP, and CTSK in wild-type and *Jdp2*$^{-/-}$ MDMs stimulated with 50 ng/ml RANKL (n = 3).

(C) Soft X-ray images of femurs.

(D) Femur lengths.

(E) BMDs of 20 longitudinal femur divisions.

(F) Representative μCT images of distal femurs (top, longitudinal view; middle, axial view of metaphyseal region; bottom, 3D view of metaphyseal region).

(G) Bone morphometric analysis of distal femurs by μCT.

a significant reduction in the osteoclast surface/bone surface ratio in *Jdp2*$^{-/-}$ mice, whereas the osteoblast surface/bone surface ratio and bone formation rate were normal (Figures 2J and 2K). Consistent with the decreased osteoclastogenesis in vivo, the serum bone resorption marker TRACP5b was lower in *Jdp2*$^{-/-}$ mice (Figure 2L). Furthermore, wild-type mice engrafted with bone marrow cells from *Jdp2*$^{-/-}$ mice had an increased bone volume phenotype (Figures S2T and S2U). Collectively, these results indicate that Jdp2 is critical for controlling osteoclastogenesis both in vitro and in vivo.

Neutrophils in *Jdp2*$^{-/-}$ Mice Are Morphologically Normal but Show Impaired Ly6G Expression

A recent report suggested that Jdp2 may be involved in the choice between lymphoid or myeloid differentiation (Ji et al., 2010). Therefore, we focused on the populations of lymphoid and myeloid cells (Figure S3A). No differences in the expressions of cell surface phenotype markers and numbers and ratios of T cells, B cells, and DCs in the spleen were observed between wild-type and *Jdp2*$^{-/-}$ mice (Figure S3A). We also checked the cytokine production (Figures S3B and S3C), bactericidal function (Figure S3D), superoxide production (Figure S3E), and phagocytosis activity (Figure S3F) in *Jdp2*$^{-/-}$ MDMs and conventional DCs (cDCs), and all phenotypes were normal.

Because Jdp2 was highly expressed in mature splenic neutrophils (Figure 1A), we compared the Jdp2 mRNA and protein expression between splenic and bone marrow neutrophils. Jdp2 expression in bone marrow mature CD11b^{+}Ly6G^{hi} neutrophils was lower than that in splenic mature CD11b^{+}Ly6G^{hi} neutrophils, but higher than that in bone marrow immature CD11b^{+}Ly6G^{lo} neutrophils (Figures S3G and S3H). These findings suggest that Jdp2 gradually increases during neutrophil differentiation and maturation.

To check the maturity of neutrophils from *Jdp2*$^{-/-}$ mice, we performed FACS analyses by using CD11b and Ly6G markers (Figure 3A). In *Jdp2*$^{-/-}$ bone marrow cells, the proportion of the CD11b^{+}Ly6G^{hi} population was shifted toward the CD11b^{+} Ly6G^{lo} population (Figure 3A). This low level of Ly6G indicated accumulation of immature cells. However, contrary to our expectation, *Jdp2*$^{-/-}$ neutrophils displayed a normal segmented nuclear morphology (Figure 3A). Because the CD11b^{+} population includes a Ly6C^{hi}Ly6G^{lo} inflammatory monocyte population (Colonna et al., 2004; Lagasse and Weissman, 1996) and a Ly6C^{lo}Ly6G^{+} neutrophil population, CD11b^{+} cells were further gated on CD11b^{+}Ly6C^{lo}Ly6G^{+} neutrophils and CD11b^{+}Ly6C^{hi} Ly6G^{lo} inflammatory monocytes to exclude monocytes from the *Jdp2*$^{-/-}$ CD11b^{+}Ly6G^{+} population (Figure 3B). Among CD11b^{+}Ly6C^{lo}Ly6G^{+} neutrophil populations, the CD11b^{+}Ly6C^{lo} Ly6G^{hi} population was shifted to the CD11b^{+}Ly6C^{lo}Ly6G^{lo} population in *Jdp2*$^{-/-}$ mice (Figure 3B). In contrast, CD11b^{+} Ly6C^{hi}Ly6G^{lo} inflammatory monocyte populations were comparable between wild-type and *Jdp2*$^{-/-}$ cells (Figure 3B). We also confirmed that both wild-type and *Jdp2*$^{-/-}$ CD11b^{+}Ly6C^{lo}Ly6G^{+} neutrophil populations had similar segmented nuclei (Figure 3B).

To further assess the abnormal bone marrow CD11b^{+} Ly6C^{lo}Ly6G^{+} neutrophil population in *Jdp2*$^{-/-}$ mice, we analyzed the cellular microstructure by transmission electron microscopy (TEM) (Figure 3C). However, the intracellular morphology of *Jdp2*$^{-/-}$ cells seemed normal (Figure 3C). To determine whether the abnormal neutrophils accumulated only in the bone marrow, we performed FACS analyses of thioglycollate-elicited peritoneal neutrophils and splenocytes (Figures 3D and 3E). An atypical CD11b^{+}Ly6C^{lo}Ly6G^{lo} population was observed in *Jdp2*$^{-/-}$ peritoneal (Figure 3D) and splenic (Figure 3E) neutrophils. To determine whether the defect in neutrophils in *Jdp2*$^{-/-}$ mice was bone marrow derived and cell intrinsic, we engrafted irradiated wild-type mice with *Jdp2*$^{-/-}$ or wild-type bone marrow. After reconstitution, we observed the same phenotype of neutrophils in the wild-type mice with *Jdp2*$^{-/-}$ bone marrow as in the *Jdp2*$^{-/-}$ mice (Figures S3O–S3Q). Together, these findings suggest that *Jdp2*$^{-/-}$ neutrophils are morphologically normal but have diminished Ly6G expression and that this abnormality arises in a cell-intrinsic manner.

Impaired Apoptosis and Bactericidal Function in *Jdp2*$^{-/-}$ Neutrophils

Intriguingly, we observed slight increases in CD11b^{+}Ly6C^{lo} Ly6G^{+} neutrophil numbers (~20%) in *Jdp2*$^{-/-}$ bone marrow and peripheral populations (Figures 3A, 3B, and 3E). Given this observation, we examined the spontaneous apoptosis of *Jdp2*$^{-/-}$ peritoneal neutrophils (Figure 3F). To our surprise, *Jdp2*$^{-/-}$ neutrophils showed impaired apoptosis compared with wild-type neutrophils (Figure 3F). Microarray and quantitative PCR (qPCR) analyses of neutrophils revealed that Bcl-2 expression was significantly increased in *Jdp2*$^{-/-}$ neutrophils, whereas Jdp2 deficiency had no effect on the diverse array of other Bcl-2-associated genes (Figures 3G–3I). Next, several assays were used to examine *Jdp2*$^{-/-}$ peritoneal neutrophil function. First, the capacity of *Jdp2*$^{-/-}$ mice to recruit neutrophils into the peritoneal cavity after thioglycollate injection was determined, with no difference in cell numbers found between wild-type and *Jdp2*$^{-/-}$ mice (Figure S3I). Second, we checked the cytokine production by *Jdp2*$^{-/-}$ neutrophils and found that Jdp2 deficiency did not alter cytokine production in response to TLR ligands (Figure S3J). Third, we analyzed the function of Jdp2 in NET formation. Intriguingly, we observed a 50% reduction in NET formation in neutrophils from *Jdp2*$^{-/-}$ mice in response to *Staphylococcus aureus* and *Candida albicans* infection (Figures 3J–3M). Fourth, because ROS, such as superoxide, are required for NET formation, we quantified superoxide production by *Jdp2*$^{-/-}$ neutrophils in

(H) Representative proximal tibias.
(I) Bone morphometric analysis of proximal tibias.
(J) TRAP staining of metaphyseal portions of tibias.
(K) Bone histomorphometric analysis of metaphyseal portions of tibias.
(L) Serum levels of TRACP5b and alkaline phosphatase (ALP).
Abbreviations: BV/TV, bone volume per tissue volume; Tb.Th, trabecular bone thickness; Tb.N, trabecular bone number; Tb.Sp, trabecular bone spacing; Oc.S/BS, osteoclast surface per bone surface; ES/BS, eroded surface per bone surface; Ob.S/BS, osteoblast surface per bone surface; BFR, bone formation rate. Error bars, SE. *$p < 0.05$; **$p < 0.01$ ($n = 4$).

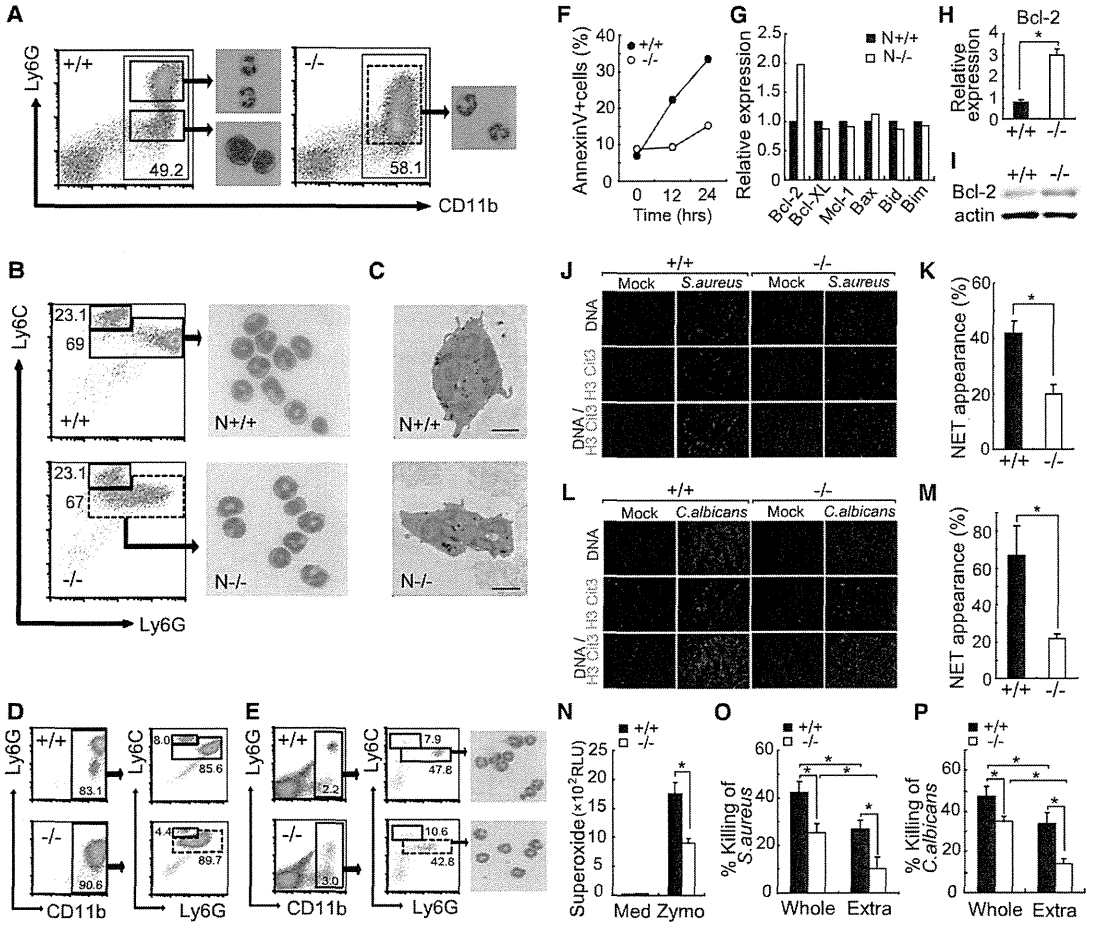

Figure 3. Abnormal Phenotype of *Jdp2*$^{-/-}$ Neutrophils

(A) FACS analysis of wild-type and *Jdp2*$^{-/-}$ bone marrow cells via Ly6G and CD11b markers. Gated cells were sorted and stained with May-Grunwald-Giemsa.

(B) CD11b^{+} populations in (A) were further analyzed with Ly6C marker. CD11b^{+}Ly6C^{lo}Ly6G^{+} neutrophils (N+/+ and N−/−) were sorted and stained as in (A).

(C) N+/+ and N−/− cells were fixed, stained with diaminobenzidine, and analyzed by TEM. Scale bars represent 2 μm.

(D and E) Peritoneal neutrophils (D) and splenocytes (E) were analyzed as in (B).

(F) Peritoneal neutrophils were cultured in vitro and analyzed for the percentage of annexin V-positive cells by FACS (n = 3 independent experiments).

(G) mRNA levels of apoptosis-regulating genes in bone marrow CD11b^{+}Ly6C^{lo}Ly6G^{+} neutrophils (N+/+ and N−/−) analyzed by a microarray.

(H and I) Bcl2 mRNA (H) and protein (I) expression levels in wild-type and *Jdp2*$^{-/-}$ peritoneal neutrophils were analyzed by qPCR and protein immunoblotting, respectively (n = 3).

(J) Peritoneal neutrophils were infected by *S. aureus* for 2 hr (MOI = 50) and stained by Hoechst and anti-histone H3 Cit3 Ab. DNA-histone H3 Cit3 Ab double-positive structures were defined as NETs.

(K) 50 microscopic fields (40×) in wells containing *S. aureus*-infected neutrophils, shown in (J), were checked and the rate of NET appearance was calculated (n = 4 observations).

(L) Peritoneal neutrophils were infected by *C. albicans* for 2 hr (MOI = 50) and stained as in (J).

(M) *C. albicans*-induced NET formation in (L) was measured as in (K).

(N) Peritoneal neutrophils were stimulated with 100 μg/ml Zymosan for 15 min and supernatant superoxide levels were measured.

(O) *S. aureus* killing by peritoneal neutrophils. Phagocytosis was inhibited by cytochalasin D and bacterial killing was measured (Extra) (n = 6).

(P) *C. albicans* killing by peritoneal neutrophils was determined as in (O).

Error bars, SE. *p < 0.05.

response to Zymosan and Curdlan. We observed 50% reductions in superoxide production in *Jdp2*$^{-/-}$ neutrophils (Figures 3N and S3L). We also checked the expression of Dectin-1, a Curdlan receptor, and observed similar expression levels between wild-type and *Jdp2*$^{-/-}$ neutrophils (Figure S3K). To clarify the mechanisms of decreased superoxide production in Jdp2 deficiency, we checked the expression levels of NADPH oxidase subunits and found that NCF1 expression was lower in *Jdp2*$^{-/-}$ neutrophils than in wild-type cells (Figure S3M). Therefore, we infected *Jdp2*$^{-/-}$ neutrophils with a retrovirus encoding NCF1 and measured the superoxide production. However, the rescue of *Jdp2*$^{-/-}$ neutrophils by NCF1 was less efficient than that by Jdp2 (Figure S3N). Thus, increased NCF1 can partially rescue the impaired superoxide production in *Jdp2*$^{-/-}$ neutrophils. Finally, to determine whether the functional defects of *Jdp2*$^{-/-}$ neutrophils were associated with bacterial killing

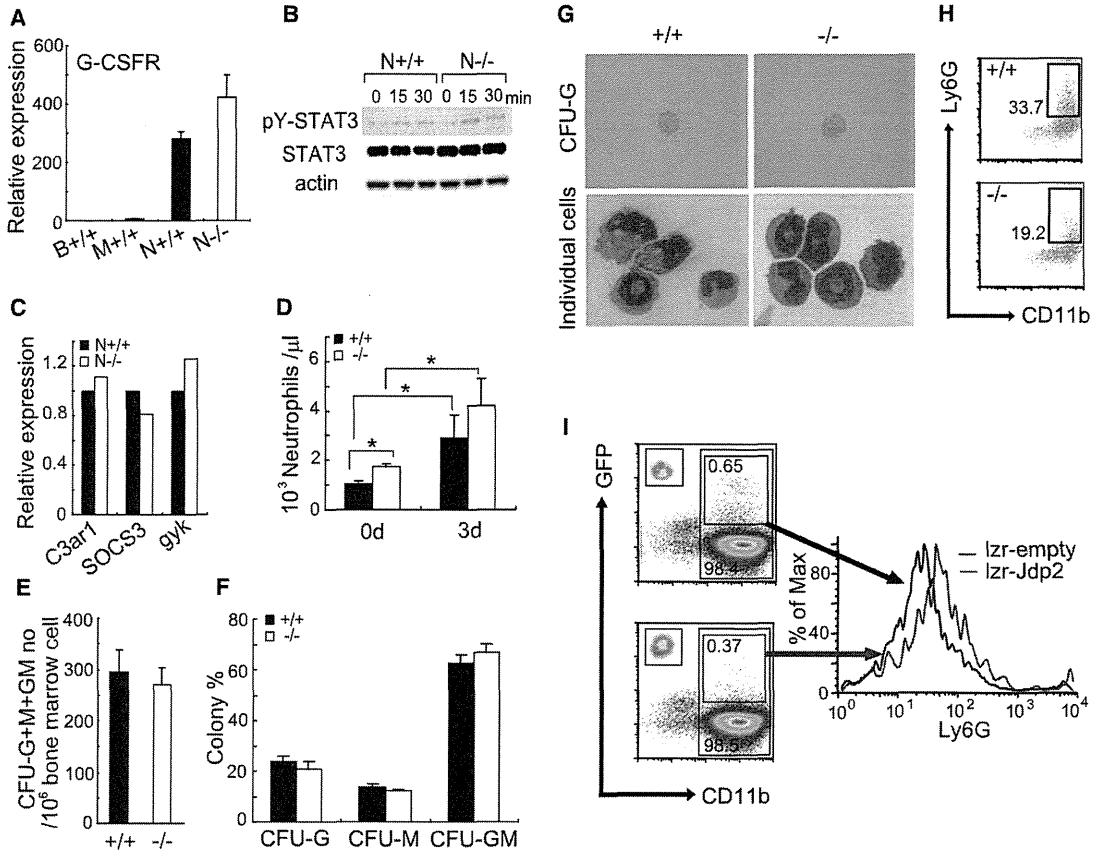

Figure 4. G-CSF Response Kinetics of *Jdp2*$^{-/-}$ Cells

(A) G-CSFR mRNA levels in wild-type and *Jdp2*$^{-/-}$ bone marrow CD11b^{+}Ly6C^{lo}Ly6G^{+} neutrophils (N+/+ and N−/−) measured by qPCR. Error bars, SE (n = 3).

(B) Cells in (A) were stimulated with 100 ng/ml G-CSF. STAT3 and pY-STAT3 levels were detected by immunoblotting.

(C) mRNA levels of STAT3 target genes in CD11b^{+}Ly6C^{lo}Ly6G^{+} neutrophils (N+/+ and N−/−) analyzed by a microarray.

(D) G-CSF (1 μg) was subcutaneously injected into wild-type and *Jdp2*$^{-/-}$ mice from days 0 to 3. At 6 hr after the last injection, blood was collected and CD11b^{+}Ly6G^{+} neutrophils were counted. Error bars, SE (n = 3). *p < 0.05.

(E and F) Bone marrow cells were cultured for 7 days in MethoCult. Total numbers of CFU-G, CFU-M, and CFU-GM colonies (E) and their rates (F) were determined. Error bars, SE (n = 6).

(G) Bone marrow cells were cultured for 7 days in MethoCult with 50 ng/ml G-CSF. Representative images of CFU-G and diaminobenzidine plus May-Grunwald-Giemsa-stained individual cells are indicated.

(H) CFU-G in (G) were collected and analyzed by FACS with CD11b and Ly6G markers.

(I) *Jdp2*$^{-/-}$ bone marrow cells were infected with a retrovirus encoding Jdp2 and GFP (Izr-Jdp2) or GFP alone (Izr-empty) with G-CSF for 9 days. CD11b^{+}GFP^{+} cells were gated and Ly6G expression levels were quantified by FACS. Gated cells were also sorted and stained by May-Grunwald-Giemsa (upper left insets in the scatter plots).

deficits, we performed in vitro killing assays with *S. aureus* and *C. albicans* (Figures 3O and 3P). Phagocytosis-dependent intracellular killing was inhibited by pretreating neutrophils with cytochalasin D. We observed that component killing mainly occurred in the extracellular space (Figures 3O and 3P) and that whole and extracellular bacterial killing by neutrophils from *Jdp2*$^{-/-}$ mice was significantly decreased compared with wild-type mice (Figures 3O and 3P). Together, these results clearly indicate that the bactericidal function is impaired in *Jdp2*$^{-/-}$ neutrophils.

Abnormal Differentiation of *Jdp2*$^{-/-}$ Neutrophils In Vitro Is Corrected by Re-expression of Jdp2

To investigate whether G-CSF signaling is altered by Jdp2 deficiency, we examined the expression levels of G-CSF receptor and STAT3. We found that G-CSF receptor (G-CSFR) expression was comparable between wild-type and *Jdp2*$^{-/-}$ neutrophils (Figure 4A), as was the expression of both STAT3 and phosphorylated STAT3 (Figure 4B). Microarray data confirmed the normal expression levels of G-CSF target genes (Figure 4C). We also counted the blood neutrophil numbers after intraperitoneal G-CSF injection and found comparable increasing rates of neutrophil numbers between wild-type and *Jdp2*$^{-/-}$ mice (Figure 4D). Thus, loss of Jdp2 does not influence G-CSF signaling.

Subsequently, we examined whether the altered differentiation of neutrophils in *Jdp2*$^{-/-}$ mice was a late-phase abnormality. *Jdp2*$^{-/-}$ bone marrow cells gave rise to the same numbers of granulocyte colony-forming units (CFU-G), granulocyte-macrophage colony-forming units (CFU-GM), and macrophage

colony-forming units (CFU-M) as did wild-type cells, with similar rates of formation (Figures 4E and 4F). We also added G-CSF to stem cell medium and cultured bone marrow cells (Figure 4G). As expected, the colony numbers (data not shown) and morphology (Figure 4G) between the two cell types were similar, but Ly6G expression was decreased in cells derived from *Jdp2*$^{-/-}$ bone marrow colonies (Figure 4H). Together, our findings imply that the abnormality in neutrophils from *Jdp2*$^{-/-}$ mice arises in the late differentiation phase and not in the initial differentiation phase.

Finally, we determined whether reintroduction of Jdp2 could rescue the terminal differentiation. We infected *Jdp2*$^{-/-}$ bone marrow cells with a retrovirus encoding Jdp2 and GFP or GFP alone and cultured the cells in medium containing G-CSF (Figure 4I). After 9 days, the cells were harvested and their Ly6G expression levels in gated GFP-positive neutrophils were quantified by FACS (Figure 4I). As expected, *Jdp2*$^{-/-}$ bone marrow-derived neutrophils infected with the Jdp2-GFP retrovirus exhibited increased Ly6G expression compared with control GFP-only cells (Figure 4I). Thus, the defect in neutrophil differentiation in *Jdp2*$^{-/-}$ mice appears to be cell autonomous and can be corrected by re-expression of Jdp2.

Primary Granule mRNA Expression Is Elevated in *Jdp2*$^{-/-}$ Neutrophils

The mRNA levels of granule genes are higher in immature neutrophils than in mature neutrophils (Martinelli et al., 2004). Therefore, we analyzed the diverse RNAs of CD11b^{+}Ly6C^{lo}Ly6G^{+} bone marrow neutrophils encoding primary, secondary, and tertiary granules by using microarray data (Figure 5A). Intriguingly, the mRNA levels for primary granule proteins, such as MPO, CTSG, and PR3, were significantly increased in *Jdp2*$^{-/-}$ neutrophils, whereas those for secondary and tertiary granule proteins were comparable to control cells (Figure 5A). The expression of other bactericidal granule proteins, such as Lipocalin2 and Cramp, was comparable (Figure S4A). We confirmed these aberrant primary granule expressions in bone marrow and peritoneal neutrophils by qPCR (Figures 5B and 5C). However, in immunoblotting analyses, the expression levels of primary granule proteins (Figure 5D) and their degranulation in response to LPS (Figure S4B) seemed comparable between wild-type and *Jdp2*$^{-/-}$ neutrophils.

To reveal the mechanism of the aberrant mRNA expression in *Jdp2*$^{-/-}$ neutrophils, we selected a set of genes whose expression levels were more abundant in *Jdp2*$^{-/-}$ neutrophils than in wild-type cells (Figure S4C) based on microarray data and examined their promoters for the presence of transcription factor binding sites. The analysis revealed that C/EBP binding sequences were highly enriched in the promoters of Jdp2-regulated genes compared with randomly selected gene promoters (Figures S4C–S4E). Further, we found that C/EBP binding sites were most enriched among 198 transcription factor binding sequences tested (Table S1). Thus, we quantified the mRNAs of the C/EBP gene family involved in myeloid differentiation. However, their expression levels were comparable (Figure 5E). C/EBPα was reported to be the master regulator of the expression of primary granule genes (Zhang et al., 1998). Therefore, we examined the DNA-binding activities of C/EBPα and C/EBPβ to their consensus oligonucleotides by using ELISA-based transcription factor kits (Figure 5F). Although the protein expression levels were again comparable (Figure 5G), C/EBPα, but not C/EBPβ, DNA binding was increased in *Jdp2*$^{-/-}$ neutrophils (Figure 5F). In addition, Jdp2 binding to the C/EBPα promoter was not detected by chromatin immunoprecipitation (ChIP) analyses (Figure 5H). When GFP-fused Jdp2 was retrovirally overexpressed in primary neutrophils, its expression was restricted to the nucleus (Figure S4F). These observations led us to examine the binding of Jdp2 to C/EBPα, and an association between C/EBPα and Jdp2 was found by immunoprecipitation (Figures 5I and 5J). From this, we examined the effect of Jdp2 on the transcriptional activity of C/EBPα (Figure 5K). For this experiment, we used a luciferase reporter plasmid driven by C/EBP transcriptional response elements. Overexpression of the C/EBPα gene only activated this promoter, whereas simultaneous expression of Jdp2 dose dependently reduced the activity of the promoter to the control level (Figure 5K). Together, these findings suggest that Jdp2 inhibits the transcriptional activity of C/EBPα by directly binding to the gene and inhibiting C/EBPα from binding to its target sequence. We also overexpressed C/EBPα in wild-type bone marrow cells and found that C/EBPα enhanced primary granule mRNAs (Figures S4G and S4H). Furthermore, when we re-expressed Jdp2 in *Jdp2*$^{-/-}$ bone marrow cells, DNA binding of C/EBPα and expression of primary granule genes were downregulated (Figures S4I and S4J). We also overexpressed C/EBPα in wild-type differentiated neutrophils (Figure S4K) and found that expression of Bcl-2 (Figure S4M) but not Ly6G (Figure S4L) was induced, leading to impaired apoptosis (Figure S4N). Together, our observations strengthen the idea that *Jdp2*$^{-/-}$ neutrophils are immature and suggest that increased primary granule and Bcl-2 mRNA expressions are attributable to increased C/EBPα activation.

ATF3 Is a Target of Jdp2 and Regulates Ly6G Expression

Among AP-1 family members, ATF3 is the closest relative of Jdp2 (Figure 6A). This information prompted us to measure ATF3 expression in neutrophils. ATF3 expression in bone marrow and peritoneal neutrophils was significantly increased (Figure 6B). We also overexpressed Jdp2 in wild-type and *Jdp2*$^{-/-}$ neutrophils and found that Jdp2 suppressed ATF3 expression (Figures 6C and 6D). Jdp2 is known to act as an epigenetic regulator of gene expression (Jin et al., 2006). Therefore, we analyzed the genome-wide status of histone acetylation, H3K4 trimethylation, and H3K27 trimethylation in wild-type and *Jdp2*$^{-/-}$ peritoneal neutrophils by using the ChIP-sequencing (ChIP-Seq) technique (Figure 6E). First, genes were chosen based on their differences in expression in wild-type and *Jdp2*$^{-/-}$ neutrophils. However, we did not find an apparent correlation between epigenetic statuses (data not shown). Moreover, primary granule genes did not have significant peaks for acetyl-histone, H3K4me3, and H3K27me3 in either wild-type or *Jdp2*$^{-/-}$ peritoneal neutrophils (Figure S5), indicating that expression of these genes is not regulated by the epigenetic status. When we focused on the ATF3 locus, we found a dramatic increase in the acetyl-histone status of the promoter region close to the transcription start site (Figure 6E). However, the same region had comparable H3K4me3 and H3K27me3 statuses (Figure 6E). By ChIP analyses, we confirmed an increase in the acetyl-histone status at the ATF3 promoter region in *Jdp2*$^{-/-}$ peritoneal neutrophils and observed

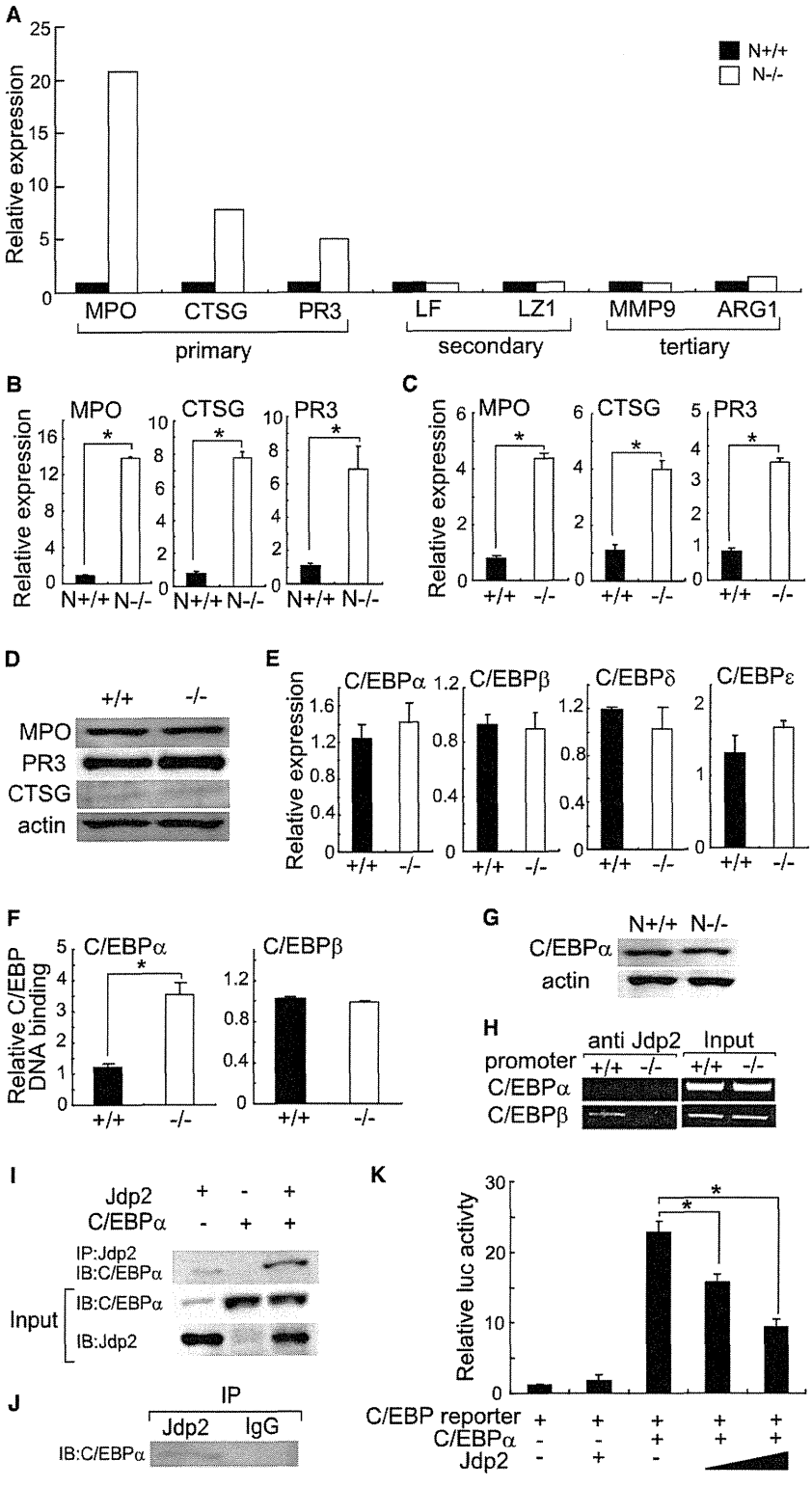

Figure 5. Aberrant mRNA Levels of Primary Granule Genes in *Jdp2*$^{-/-}$ Neutrophils

(A) Primary, secondary, and tertiary granule mRNA levels in bone marrow CD11b^{+}Ly6C^{lo}Ly6G^{+} neutrophils (N+/+ and N−/−) analyzed by a microarray.

(B and C) MPO, CTSG, and PR3 mRNA levels in CD11b^{+}Ly6C^{lo}Ly6G^{+} neutrophils (N+/+ and N−/−) (B) and peritoneal neutrophils (C) measured by qPCR.

(D) Primary granule protein levels in peritoneal neutrophils from wild-type and *Jdp2*$^{-/-}$ mice.

(E) C/EBP gene family mRNA levels in peritoneal neutrophils from wild-type and *Jdp2*$^{-/-}$ mice measured by qPCR.

(F) DNA-binding activities of C/EBPα and C/EBPβ in wild-type and *Jdp2*$^{-/-}$ peritoneal neutrophils measured with a TransAM Transcription Factor Assay Kit.

(G) C/EBPα protein levels in nuclear extracts from wild-type and *Jdp2*$^{-/-}$ peritoneal neutrophils analyzed by immunoblotting.

(H) ChIP analyses with a Jdp2 Ab of lysates from wild-type and *Jdp2*$^{-/-}$ peritoneal neutrophils. C/EBPα and C/EBPβ promoter regions were detected by PCR.

(I) 293T cells were transfected with the indicated pCMV expression vectors. After anti-Jdp2 immunoprecipitation (IP), input and immunoprecipitates were analyzed by immunoblotting with C/EBPα and Jdp2 Abs.

(J) Wild-type peritoneal neutrophils were lysed. After anti-Jdp2 and control IgG IP, immunoprecipitates were analyzed by immunoblotting with a C/EBPα Ab.

(K) Luciferase assays examining the effects of Jdp2 on the transcriptional activity of C/EBPα.

Error bars, SE (n = 3). *p < 0.05.

direct binding between Jdp2 and the ATF3 promoter (Figure 6F). Furthermore, we found that Jdp2 overexpression in wild-type neutrophils suppressed ATF3 promoter acetylation (Figure 6G).

Finally, to determine whether increased ATF3 expression affected neutrophil differentiation, we infected wild-type bone marrow cells with a retrovirus encoding ATF3 and GFP or GFP alone and analyzed the cells by FACS after 5 days as described earlier. Intriguingly, neutrophils infected with the ATF3-GFP retrovirus showed decreased Ly6G expression levels but unchanged cellular morphology, compared with GFP-alone control cells (Figure 6H). Thus, ATF3 is a negative regulator of neutrophil differentiation, and its expression is strictly regulated by Jdp2.

Jdp2$^{-/-}$ Mice Are Highly Susceptible to Bacterial and Fungal Infection

Because decreased neutrophil function is an important risk factor for *C. albicans* infection, we checked the susceptibility of *Jdp2*$^{-/-}$ mice to *C. albicans* challenge (Figures 7A–7C). We observed a slight but significant increase in *C. albicans* susceptibility in *Jdp2*$^{-/-}$

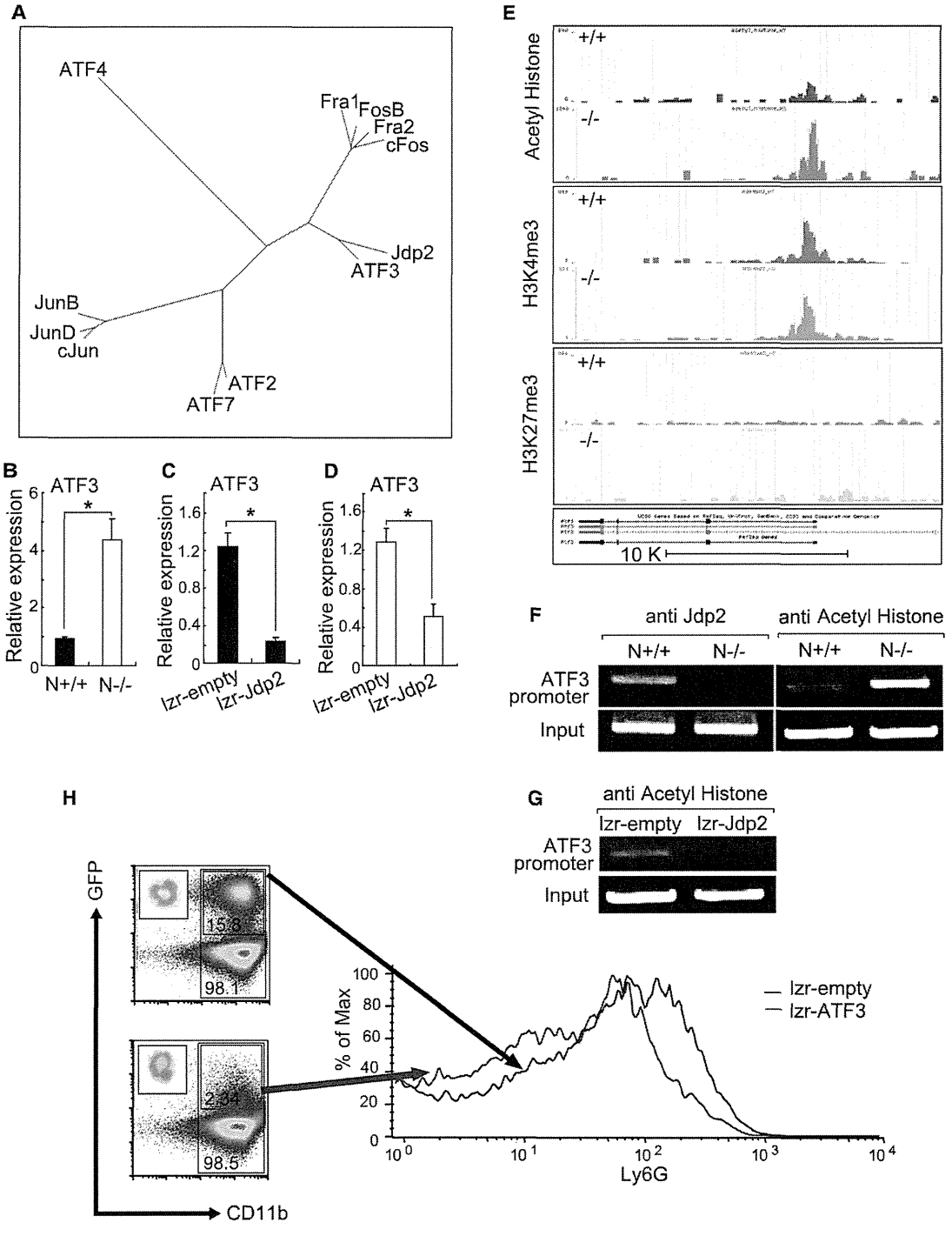

Figure 6. ATF3 Is a Target of Jdp2 and Modulates Ly6G Surface Expression

(A) Phylogenetic tree for AP-1 family proteins and Jdp2.

(B) ATF3 mRNA levels in bone marrow CD11b^{+}Ly6C^{lo}Ly6G^{+} neutrophils (N+/+ and N−/−) analyzed by qPCR.

(C and D) Wild-type (C) and *Jdp2*$^{-/-}$ (D) bone marrow cells were infected with a retrovirus encoding Jdp2 and GFP (Izr-Jdp2) or GFP alone (Izr-empty) and cultured with G-CSF. After 5 days, the cells were harvested and CD11b^{+}GFP^{+} cells were sorted. ATF3 mRNA levels were measured by qPCR.

(E) ChIP-seq enrichment profiles for acetyl-histone, H3K4me3, and H3K27me3 at the ATF3 locus in wild-type and *Jdp2*$^{-/-}$ peritoneal neutrophils.

(F) ChIP analyses with Jdp2 and acetyl-histone Abs of lysates from wild-type and *Jdp2*$^{-/-}$ bone marrow CD11b^{+}Ly6C^{lo}Ly6G^{+} neutrophils (N+/+ and N−/−). DNA fragments of the ATF3 promoter region were detected by PCR.

(G) ChIP analyses with an acetyl-histone Ab of lysates in (C). DNA fragments of the ATF3 promoter region were detected by PCR.

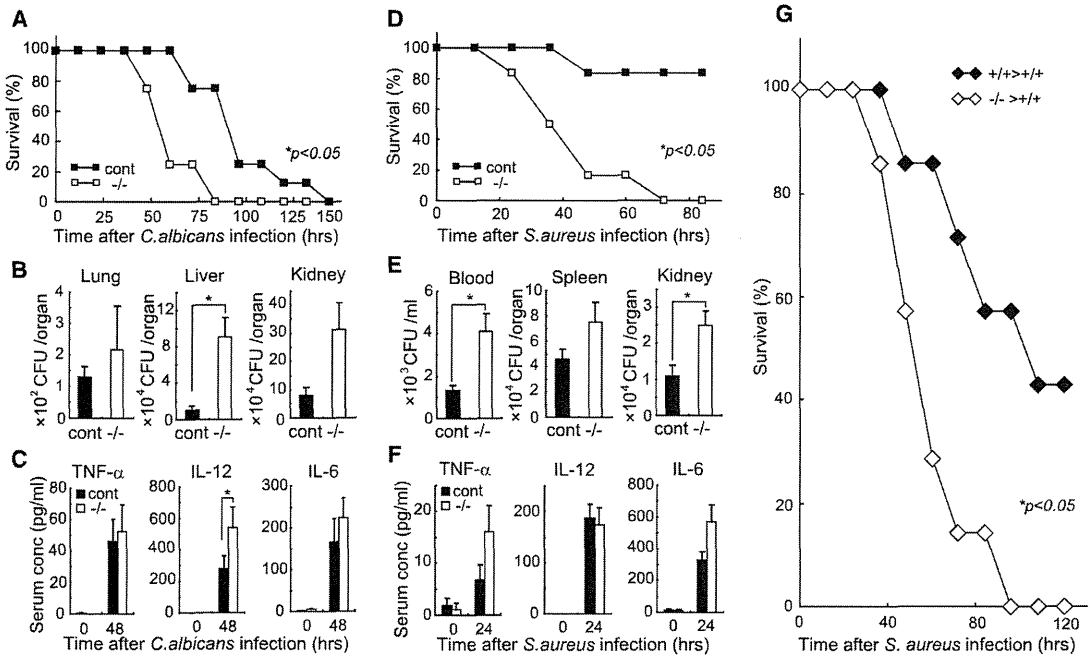

Figure 7. *Jdp2*$^{-/-}$ Mice Are Susceptible to Infection

(A–C) *C. albicans* was intravenously injected into *Jdp2*$^{+/+}$*Jdp2*$^{+/-}$ mice (control, n = 8) and *Jdp2*$^{-/-}$ mice (−/−, n = 8) and the mice were monitored (A). *Jdp2*$^{-/-}$ mice showed significantly worse survival than control mice ($p < 0.05$). CFU in the indicated organs (B) and serum cytokine levels (C) were determined at 36 hr after infection.

(D–F) *S. aureus* was intravenously injected into *Jdp2*$^{+/+}$*Jdp2*$^{+/-}$ mice (control, n = 6) and *Jdp2*$^{-/-}$ mice (−/−, n = 6) and the mice were monitored (D). *Jdp2*$^{-/-}$ mice showed significantly worse survival than control mice ($p < 0.05$). CFU in the indicated organs (E) and serum cytokine levels (F) were determined at 36 hr after infection.

(G) *S. aureus* was intravenously injected into wild-type mice reconstituted by transplantation of wild-type (+/+ > +/+, n = 7) or *Jdp2*$^{-/-}$ (−/− > +/+, n = 7) bone marrow and the mice were monitored. The survival was significantly worse in −/− > +/+ mice than in +/+ > +/+ mice ($p < 0.05$).

Error bars, SE (n = 4 unless indicated). *$p < 0.05$.

mice (Figure 7A), which showed elevated numbers of *C. albicans* CFU in their liver compared with wild-type mice (Figure 7B). The serum IL-12 levels were significantly elevated in *Jdp2*$^{-/-}$ mice, compared with wild-type mice, but the serum TNF-α and IL-6 levels were comparable (Figure 7C). We also infected *Jdp2*$^{-/-}$ and wild-type mice with *S. aureus* (Figures 7D–7F). Surprisingly, *Jdp2*$^{-/-}$ mice were highly susceptible to *S. aureus* infection, compared with wild-type mice (Figure 7D). *Jdp2*$^{-/-}$ mice showed significantly elevated numbers of *S. aureus* CFU in their blood and kidneys, compared with wild-type mice (Figure 7E). In contrast, the serum cytokine levels were not significantly altered (Figure 7F). To evaluate the relevance of hematopoietic Jdp2 deficiency to protective immunity against pathogens, we irradiated wild-type mice and reconstituted them with bone marrow from wild-type or *Jdp2*$^{-/-}$ mice (Figure 7G). Chimeric mice lacking Jdp2 in their hematopoietic system showed significantly increased susceptibility to *S. aureus* (Figure 7G). To evaluate the importance of lymphocytes in protective immunity against *S. aureus* infection in our experimental model, we depleted T and B cells in wild-type mice reconstituted with bone marrow from wild-type mice by using CD3 and CD20 Abs (Figure S6A). However, this depletion had no effect on survival in response to *S. aureus* (Figure S6B). Thus, we think our infection model reflects the function of cells other than T and B cells. Next, we depleted neutrophils in bone marrow chimeric mice by using a Ly6G Ab (Figure S6C). We infected the neutrophil-depleted chimeric mice with *S. aureus* and observed no significant difference in *S. aureus*-induced lethality between wild-type and *Jdp2*$^{-/-}$ chimeric mice (Figure S6D). Thus, these findings suggest that the increased susceptibility to *S. aureus* in *Jdp2*$^{-/-}$ mice is due to an abnormal neutrophil phenotype.

DISCUSSION

We have demonstrated that Jdp2 plays a critical role in osteoclastogenesis in vivo. We also discovered that in vitro osteoclastogenesis was completely abolished in *Jdp2*$^{-/-}$ cells. Furthermore, RANKL-mediated Jdp2 induction appeared to be

(H) Wild-type bone marrow cells were infected with a retrovirus encoding ATF3 and GFP (Izr-ATF3) or GFP alone (Izr-empty) and cultured with G-CSF. After 5 days, CD11b^{+}GFP^{+} cells were gated and Ly6G expression levels were quantified by FACS. Gated cells were also sorted and stained by May-Grunwald-Giemsa (upper left insets in the scatter plots).

Error bars, SE (n = 3). *$p < 0.05$.

regulated through c-Fos. NFATc1 activation was partially suppressed, meaning that Jdp2 may also positively regulate its activity. However, we did not detect a direct association between Jdp2 and NFATc1 (data not shown), and Jdp2 had no effect on NFATc1 binding to its promoter region. Thus, indirect mechanisms are likely to modulate the NFATc1 activity.

The defect in osteoclastogenesis in *Jdp2*$^{-/-}$ mice in vivo was relatively mild compared with its effect on in vitro osteoclastogenesis. It has been reported that calcium signaling is important for NFATc1 activation and that such costimulatory signaling is supported by ITAM-harboring adaptors, such as FcRγ and DNAX-activation protein 12 (DAP12) (Koga et al., 2004). Because RANKL-induced calcium oscillation was normal in *Jdp2*$^{-/-}$ cells in this study, signaling through ITAM-harboring molecules is likely to be normal. These findings further suggest that another unknown costimulatory signaling pathway may be compensating for the Jdp2 deficiency in vivo. Further studies are needed to explore the role of Jdp2 in osteoclasts, but our data provide insights into c-Fos-Jdp2 axis-mediated osteoclastogenesis and suggest a basis for the possibility of Jdp2-targeted therapeutic approaches to treat osteoporosis.

Our present data clearly revealed an unexpected and strict requirement for Jdp2 in proper differentiation of neutrophils. *Jdp2*$^{-/-}$ neutrophils were morphologically normal but had impaired surface expression of Ly6G, apoptosis, and bactericidal function. Furthermore, C/EBPα activation and expression of Bcl-2 and primary granule genes were increased. Our data also suggest that Jdp2 suppresses C/EBPα by directly binding to it. Notably, *Jdp2*$^{-/-}$ neutrophils showed normal primary granule protein levels but increased mRNA levels. Similar discrepancies have been reported in several knockout mice. For example, Gfi1-deficient neutrophils exhibit immature morphology and significant increases in mRNAs, such as primary granule genes and C/EBPα, but lack granules (Hock et al., 2003). Meanwhile, Ikaros-deficient neutrophils have impaired Ly6G levels but normal granule and nuclear morphology, whereas secondary granule mRNAs seem to be increased (Dumortier et al., 2003). Thus, increased mRNA levels of granule genes can be considered a leading indicator for obstruction of differentiation. Unfortunately, we cannot explain why the granule mRNA and protein levels are dissociated in neutrophils. One hypothetical explanation is that there are insufficient amounts of translational components for granule synthesis in *Jdp2*$^{-/-}$ neutrophils.

Jdp2 is homologous to ATF3, a negative regulator of TLR signaling, and ATF3 expression is suppressed by Jdp2 in fibroblasts (Weidenfeld-Baranboim et al., 2009). Our genome-wide analysis revealed that the ATF3 promoter region was highly acetylated in *Jdp2*$^{-/-}$ neutrophils. Furthermore, we discovered that Jdp2 directly binds to the ATF3 promoter in neutrophils. Importantly, ATF3 may function as a novel negative regulator of Ly6G. We also revealed that *Jdp2*$^{-/-}$ mice are highly susceptible to infection. The impaired NET formation and ROS production in *Jdp2*$^{-/-}$ neutrophils may be responsible for the increased susceptibility to infection in *Jdp2*$^{-/-}$ mice. Intriguingly, this defect in the in vitro bactericidal function of *Jdp2*$^{-/-}$ neutrophils was mild compared with the highly impaired resistance to *S. aureus* infection. We cannot completely exclude the possibility of defects in other immune cells. Thus, our data suggest the importance of Jdp2 in host defense and also enhance curiosity to clarify the importance of Jdp2 in a wide range of hematopoietic cell functions.

Taken together, we have identified Jdp2 as a critical "osteo-innate-immunological" regulator both in vivo and in vitro. Thus, Jdp2-mediated gene regulation may be a critical target for the development of therapeutics to control abnormal neutrophil- and osteoclast-associated diseases.

EXPERIMENTAL PROCEDURES

Mice, Cells, and Reagents

The generation of *Jdp2*$^{-/-}$ mice is described in the Supplemental Experimental Procedures. Mice were housed in specific-pathogen-free conditions and all animal experiments were carried out with the approval of the animal research committee of the Research Institute for Microbial Diseases (Osaka University). Peritoneal neutrophils were prepared as described (Bertram et al., 2012). B and T cells were isolated from splenocytes with anti-B220 and anti-Thy-1.2 magnetic beads (Miltenyi Biotec), respectively. Splenic dendritic cells (DCs) were isolated with anti-CD11c magnetic beads (Miltenyi Biotec). Primary osteoclasts are prepared as described (Takegahara et al., 2006). Splenic- or bone marrow-derived CD11b^{+}F4/80^{+} macrophages and CD11b^{+}Ly6C^{lo}Ly6G^{+} neutrophils were sorted with a FACSAria (BD Biosciences). Conventional dendritic cells (cDCs) were prepared as described (Kato et al., 2005). *S. aureus* 834 was kindly provided by A. Nakane (Hirosaki University, School of Medicine, Aomori, Japan). This strain was cultured on tryptic soy broth agar plates at 37°C for 24 hr before use. *C. albicans* THK519 was obtained from a patient admitted to Tohoku University Hospital (Sendai, Japan). These cells were cultured on potato dextrose agar (PDA) plates (Eiken) at 30°C for 72 hr before use. The pathogen-associated molecular patterns (PAMPs), Abs, and ELISA kits listed in the Supplemental Experimental Procedures were purchased. Phagocytosis was quantified with a phagocytosis assay kit (500290; Cayman Chemical Company). Superoxide and apoptosis levels were measured with a Diogenes Cellular Luminescence Enhancement System (National Diagnostics) and annexin V-indocarbocyanine (BioVision), respectively.

Analysis of Osteoclastogenesis and Bone Phenotype

For in vitro osteoclast culture, MDMs were generated as described (Maruyama et al., 2006). MDMs were induced to differentiate into osteoclasts in the presence of 25 ng/ml M-CSF and various concentrations of RANKL (R&D Systems). After 3 days, TRAP staining was performed as described (Zhao et al., 2006). For pit assays, MDMs were cultured on bone resorption assay plates (Iwai Chemical Company) with 50 ng/ml RANKL. After 5 days, the plates were immersed in 1 M NH_4OH for 3 hr, and the resorption pits were counted. The in vivo bone phenotype was analyzed as described in the Supplemental Experimental Procedures.

Bone Marrow Transfer

Bone marrow transplantation was performed as described in the Supplemental Experimental Procedures.

qPCR

RNA was extracted from cells with TRIzol (Invitrogen Life Science Technologies), and reverse transcription was performed with ReverTra Ace (Toyobo Co. Ltd.). qPCR was performed in an ABI PRISM 7500 with TaqMan Assay-on-demand primers (Applied Biosystems).

Viral Gene Transfer and RNA Interference

Retroviral or lentiviral gene transfer was performed as described in the Supplemental Experimental Procedures. A siRNA for c-Fos (Stealth RNAi siRNA, MSS247212; Invitrogen) and a control oligo (Stealth RNAi siRNA, negative control Med GC; Invitrogen) were introduced into MDMs with Lipofectamine 2000 (Invitrogen) according to the manufacturer's protocols.

Immunoblotting and Immunoprecipitation

Immunoblotting and immunoprecipitation were performed as described (Kawagoe et al., 2009).

Luciferase Reporter Assay

A C/EBP reporter kit (CCS-001L; QIAGEN) and NFAT reporter kit (CCS-015L; QIAGEN) were used for transient transfection into HEK293 cells with Lipofectamine 2000. Luciferase activities were measured with a Dual-Luciferase Reporter Assay System (Promega), as described (Iwasaki et al., 2011).

Intracellular Calcium Imaging

MDMs were plated on poly-L-lysine-coated glass-bottom dishes and loaded with 5 μM Fura-2/AM for 30 min in loading solution (115 mM NaCl, 5.4 mM KCl, 1 mM $MgCl_2$, 2 mM $CaCl_2$, 20 mM HEPES, 10 mM glucose [pH 7.42]). Fura-2 fluorescent images were analyzed as described (Kuroda et al., 2008).

Immunostaining, FACS, and TEM

Immunostaining of in vitro cultured peritoneal neutrophils was performed essentially as described (Li et al., 2010). Peritoneal neutrophils were stimulated by *S. aureus* or *C. albicans* for 2 hr (MOI = 50) and stained with Hoechst and anti-histone H3 Cit3 Ab (Abcam). Abs for FACS were purchased from BD Biosciences and used for cell staining. Data were acquired in a FACSCalibur (BD Biosciences) and analyzed with FlowJo (Ashland). TEM was performed as described in the Supplemental Experimental Procedures.

Colony Assay

Bone marrow cells were cultured with MethoCult (GFM3434; Stem Cell Technologies) with or without G-CSF (50 ng/ml) supplementation, according to the manufacturer's protocol. After 7 days, the numbers of CFU-G, CFU-M, and CFU-GM were counted.

Microarray, ChIP, and ChIP-seq Analyses

The microarray, ChIP, and ChIP-seq protocols and data analyses are described in the Supplemental Experimental Procedures.

In Vitro and In Vivo Infection

In vitro bacterial killing assays were performed as described in the Supplemental Experimental Procedures. For in vivo infection, *S. aureus* was cultured in tryptic soy broth for 15 hr at 37°C. Cells were collected and suspended in PBS. Mice were infected intravenously with 0.2 ml of solution containing 3×10^7 *S. aureus* cells. *C. albicans* were collected from PDA plates and suspended in PBS. Mice were infected intravenously with 0.2 ml of solution containing 2.5×10^5 *C. albicans* cells. The numbers of viable bacteria in various organs were determined as described (Maruyama et al., 2007).

Statistical Analysis

Student's t test was used to evaluate the significance of differences, with significance set at $p < 0.05$. For survival curves, two groups were compared with a log-rank test.

ACCESSION NUMBERS

The microarray data are available in the Gene Expression Omnibus (GEO) database (http://www.ncbi.nlm.nih.gov/gds) under the accession number GSE42063.

SUPPLEMENTAL INFORMATION

Supplemental Information includes Supplemental Experimental Procedures, six figures, and one table and can be found with this article online at http://dx.doi.org/10.1016/j.immuni.2012.08.022.

ACKNOWLEDGMENTS

We thank S. Tartey and D. Ori for technical advice; E. Kamada and M. Kageyama for secretarial assistance; K. Nojima, Y. Fujiwara, and M. Kumagai for technical assistance; and T. Kawai and Y. Kumagai for fruitful discussions. This work was supported by Special Coordination Funds of the Japanese Ministry of Education, Culture, Sports, Science, and Technology, grants from the Ministry of Health, Labour, and Welfare of Japan, the Japan Society for the Promotion of Science (JSPS) through the Funding Program for World-Leading Innovative R&D on Science and Technology (FIRST Program), and a research fellowship from the JSPS for the Promotion of Science for Young Scientists. K.M. designed and performed most of the experiments. M.F., T.S., T. Kawasaki, T. Kondo, H.K., N.T., and O.T. contributed the immunological experiments. A.V. and D.S. analyzed the ChIP-seq data. K.K.Y. provided the Jdp2 antibody. The manuscript was written by K.M. S.A. supervised the overall research.

Received: May 11, 2012
Accepted: August 16, 2012
Published online: November 29, 2012

REFERENCES

Aronheim, A., Zandi, E., Hennemann, H., Elledge, S.J., and Karin, M. (1997). Isolation of an AP-1 repressor by a novel method for detecting protein-protein interactions. Mol. Cell. Biol. *17*, 3094–3102.

Bertram, A., Zhang, H., von Vietinghoff, S., de Pablo, C., Haller, H., Shushakova, N., and Ley, K. (2012). Protein kinase C-θ is required for murine neutrophil recruitment and adhesion strengthening under flow. J. Immunol. *188*, 4043–4051.

Borregaard, N., and Cowland, J.B. (1997). Granules of the human neutrophilic polymorphonuclear leukocyte. Blood *89*, 3503–3521.

Borregaard, N., Sørensen, O.E., and Theilgaard-Mönch, K. (2007). Neutrophil granules: a library of innate immunity proteins. Trends Immunol. *28*, 340–345.

Brinkmann, V., Reichard, U., Goosmann, C., Fauler, B., Uhlemann, Y., Weiss, D.S., Weinrauch, Y., and Zychlinsky, A. (2004). Neutrophil extracellular traps kill bacteria. Science *303*, 1532–1535.

Colonna, M., Trinchieri, G., and Liu, Y.J. (2004). Plasmacytoid dendritic cells in immunity. Nat. Immunol. *5*, 1219–1226.

Dumortier, A., Kirstetter, P., Kastner, P., and Chan, S. (2003). Ikaros regulates neutrophil differentiation. Blood *101*, 2219–2226.

Forman, H.J., and Thomas, M.J. (1986). Oxidant production and bactericidal activity of phagocytes. Annu. Rev. Physiol. *48*, 669–680.

Hestdal, K., Ruscetti, F.W., Ihle, J.N., Jacobsen, S.E., Dubois, C.M., Kopp, W.C., Longo, D.L., and Keller, J.R. (1991). Characterization and regulation of RB6-8C5 antigen expression on murine bone marrow cells. J. Immunol. *147*, 22–28.

Hock, H., Hamblen, M.J., Rooke, H.M., Traver, D., Bronson, R.T., Cameron, S., and Orkin, S.H. (2003). Intrinsic requirement for zinc finger transcription factor Gfi-1 in neutrophil differentiation. Immunity *18*, 109–120.

Huang, Y.C., Saito, S., and Yokoyama, K.K. (2010). Histone chaperone Jun dimerization protein 2 (JDP2): role in cellular senescence and aging. Kaohsiung J. Med. Sci. *26*, 515–531.

Humphrey, M.B., Daws, M.R., Spusta, S.C., Niemi, E.C., Torchia, J.A., Lanier, L.L., Seaman, W.E., and Nakamura, M.C. (2006). TREM2, a DAP12-associated receptor, regulates osteoclast differentiation and function. J. Bone Miner. Res. *21*, 237–245.

Iwasaki, H., Takeuchi, O., Teraguchi, S., Matsushita, K., Uehata, T., Kuniyoshi, K., Satoh, T., Saitoh, T., Matsushita, M., Standley, D.M., and Akira, S. (2011). The IκB kinase complex regulates the stability of cytokine-encoding mRNA induced by TLR-IL-1R by controlling degradation of regnase-1. Nat. Immunol. *12*, 1167–1175.

Ji, H., Ehrlich, L.I., Seita, J., Murakami, P., Doi, A., Lindau, P., Lee, H., Aryee, M.J., Irizarry, R.A., Kim, K., et al. (2010). Comprehensive methylome map of lineage commitment from haematopoietic progenitors. Nature *467*, 338–342.

Jin, C., Ugai, H., Song, J., Murata, T., Nili, F., Sun, K., Horikoshi, M., and Yokoyama, K.K. (2001). Identification of mouse Jun dimerization protein 2 as a novel repressor of ATF-2. FEBS Lett. *489*, 34–41.

Jin, C., Kato, K., Chimura, T., Yamasaki, T., Nakade, K., Murata, T., Li, H., Pan, J., Zhao, M., Sun, K., et al. (2006). Regulation of histone acetylation and nucleosome assembly by transcription factor JDP2. Nat. Struct. Mol. Biol. *13*, 331–338.

Karsenty, G., and Wagner, E.F. (2002). Reaching a genetic and molecular understanding of skeletal development. Dev. Cell *2*, 389–406.

Kato, H., Sato, S., Yoneyama, M., Yamamoto, M., Uematsu, S., Matsui, K., Tsujimura, T., Takeda, K., Fujita, T., Takeuchi, O., and Akira, S. (2005). Cell type-specific involvement of RIG-I in antiviral response. Immunity *23*, 19–28.

Kawagoe, T., Takeuchi, O., Takabatake, Y., Kato, H., Isaka, Y., Tsujimura, T., and Akira, S. (2009). TANK is a negative regulator of Toll-like receptor signaling and is critical for the prevention of autoimmune nephritis. Nat. Immunol. *10*, 965–972.

Kawaida, R., Ohtsuka, T., Okutsu, J., Takahashi, T., Kadono, Y., Oda, H., Hikita, A., Nakamura, K., Tanaka, S., and Furukawa, H. (2003). Jun dimerization protein 2 (JDP2), a member of the AP-1 family of transcription factor, mediates osteoclast differentiation induced by RANKL. J. Exp. Med. *197*, 1029–1035.

Koga, T., Inui, M., Inoue, K., Kim, S., Suematsu, A., Kobayashi, E., Iwata, T., Ohnishi, H., Matozaki, T., Kodama, T., et al. (2004). Costimulatory signals mediated by the ITAM motif cooperate with RANKL for bone homeostasis. Nature *428*, 758–763.

Kuroda, Y., Hisatsune, C., Nakamura, T., Matsuo, K., and Mikoshiba, K. (2008). Osteoblasts induce Ca2+ oscillation-independent NFATc1 activation during osteoclastogenesis. Proc. Natl. Acad. Sci. USA *105*, 8643–8648.

Lagasse, E., and Weissman, I.L. (1996). Flow cytometric identification of murine neutrophils and monocytes. J. Immunol. Methods *197*, 139–150.

Li, P., Li, M., Lindberg, M.R., Kennett, M.J., Xiong, N., and Wang, Y. (2010). PAD4 is essential for antibacterial innate immunity mediated by neutrophil extracellular traps. J. Exp. Med. *207*, 1853–1862.

Lieschke, G.J., Grail, D., Hodgson, G., Metcalf, D., Stanley, E., Cheers, C., Fowler, K.J., Basu, S., Zhan, Y.F., and Dunn, A.R. (1994). Mice lacking granulocyte colony-stimulating factor have chronic neutropenia, granulocyte and macrophage progenitor cell deficiency, and impaired neutrophil mobilization. Blood *84*, 1737–1746.

Martinelli, S., Urosevic, M., Daryadel, A., Oberholzer, P.A., Baumann, C., Fey, M.F., Dummer, R., Simon, H.U., and Yousefi, S. (2004). Induction of genes mediating interferon-dependent extracellular trap formation during neutrophil differentiation. J. Biol. Chem. *279*, 44123–44132.

Maruyama, K., Takada, Y., Ray, N., Kishimoto, Y., Penninger, J.M., Yasuda, H., and Matsuo, K. (2006). Receptor activator of NF-kappa B ligand and osteoprotegerin regulate proinflammatory cytokine production in mice. J. Immunol. *177*, 3799–3805.

Maruyama, K., Sano, G., Ray, N., Takada, Y., and Matsuo, K. (2007). c-Fos-deficient mice are susceptible to *Salmonella enterica serovar Typhimurium* infection. Infect. Immun. *75*, 1520–1523.

Nishikawa, K., Nakashima, T., Hayashi, M., Fukunaga, T., Kato, S., Kodama, T., Takahashi, S., Calame, K., and Takayanagi, H. (2010). Blimp1-mediated repression of negative regulators is required for osteoclast differentiation. Proc. Natl. Acad. Sci. USA *107*, 3117–3122.

Nishinaka, Y., Arai, T., Adachi, S., Takaori-Kondo, A., and Yamashita, K. (2011). Singlet oxygen is essential for neutrophil extracellular trap formation. Biochem. Biophys. Res. Commun. *413*, 75–79.

Takayanagi, H. (2007). Osteoimmunology: shared mechanisms and crosstalk between the immune and bone systems. Nat. Rev. Immunol. *7*, 292–304.

Takegahara, N., Takamatsu, H., Toyofuku, T., Tsujimura, T., Okuno, T., Yukawa, K., Mizui, M., Yamamoto, M., Prasad, D.V., Suzuki, K., et al. (2006). Plexin-A1 and its interaction with DAP12 in immune responses and bone homeostasis. Nat. Cell Biol. *8*, 615–622.

Weidenfeld-Baranboim, K., Hasin, T., Darlyuk, I., Heinrich, R., Elhanani, O., Pan, J., Yokoyama, K.K., and Aronheim, A. (2009). The ubiquitously expressed bZIP inhibitor, JDP2, suppresses the transcription of its homologue immediate early gene counterpart, ATF3. Nucleic Acids Res. *37*, 2194–2203.

Yamanaka, R., Barlow, C., Lekstrom-Himes, J., Castilla, L.H., Liu, P.P., Eckhaus, M., Decker, T., Wynshaw-Boris, A., and Xanthopoulos, K.G. (1997). Impaired granulopoiesis, myelodysplasia, and early lethality in CCAAT/enhancer binding protein epsilon-deficient mice. Proc. Natl. Acad. Sci. USA *94*, 13187–13192.

Zhang, P., Iwama, A., Datta, M.W., Darlington, G.J., Link, D.C., and Tenen, D.G. (1998). Upregulation of interleukin 6 and granulocyte colony-stimulating factor receptors by transcription factor CCAAT enhancer binding protein alpha (C/EBP alpha) is critical for granulopoiesis. J. Exp. Med. *188*, 1173–1184.

Zhao, C., Irie, N., Takada, Y., Shimoda, K., Miyamoto, T., Nishiwaki, T., Suda, T., and Matsuo, K. (2006). Bidirectional ephrinB2-EphB4 signaling controls bone homeostasis. Cell Metab. *4*, 111–121.

Oncogene (2013) 32, 414–421

www.nature.com/onc

ORIGINAL ARTICLE

microRNA-125b inhibits tube formation of blood vessels through translational suppression of VE-cadherin

F Muramatsu[1,3], H Kidoya[1,3], H Naito[1], S Sakimoto[1] and N Takakura[1,2]

Angiogenesis is controlled positively or negatively by extrinsic and intrinsic molecular cues in endothelial cells (ECs); in the tumor microenvironment, the action of positive regulators exceeds that of negative regulators. Thus, overinduction of negative regulators may inhibit tumor angiogenesis. MicroRNAs (miRNAs or miRs) are endogenous short noncoding RNAs regulating gene expression either through translational inhibition or destabilization of target mRNA. Here, we show that miR-125b expression is transiently induced in ECs on stimulation with vascular endothelial growth factor or by ischemia. miR-125b inhibits translation of *vascular endothelial (VE)-cadherin* mRNA and *in vitro* tube formation by ECs. Injection of miR-125b into the tumor inhibited VE-cadherin expression by ECs and induced nonfunctional blood vessel formation, resulting in inhibition of tumor growth. It has been suggested that pro-angiogenic signals in ECs also upregulate anti-angiogenic molecules simultaneously via negative feedback. Because miR-125b induction in ECs is transient after pro-angiogenic stimulation, prolonged overexpression of miR-125b could result in blood vessel regression. Thus, miR-125b may be useful in cancer therapy by causing the collapse of the lumen of ECs.

Oncogene (2013) **32,** 414–421; doi:10.1038/onc.2012.68; published online 5 March 2012

Keywords: microRNA; mir125b; angiogenesis; VE-cadherin

INTRODUCTION

In the initial step of angiogenesis, mural cells overlying endothelial cells (ECs) dissociate from them, and the ECs start to migrate and proliferate.[1] Therefore, at the onset of angiogenesis, regulators associated with blood vessel maintenance need to be transiently suppressed. ECs proliferate on stimulation with growth factors, especially vascular endothelial growth factor (VEGF), while simultaneously such factors induce upregulation of molecular cues that disrupt blood vessel stability.[2] However, expression of such molecules does not persist for the whole period of growth and maturation of blood vessels during angiogenesis.

For stabilization of blood vessels under normoxia, mural cells such as pericytes or vascular smooth muscle cells must adhere to ECs. This process of mural cell recruitment is triggered mainly by platelet-derived growth factor-B produced by ECs.[3] Subsequently, angiopoietin-1 (Ang1) produced by mural cells directly stimulates Tie2, a tyrosine kinase receptor expressed on ECs, resulting in cell-to-cell adhesion between mural cells and ECs.[4–7] Under hypoxia, for induction of angiogenic switching in pre-existing blood vessels, Ang2, an antagonist of Ang1 produced by ECs, inhibits phosphorylation of Tie2, followed by mural cell dissociation from ECs.[8] This process is thought to be essential for initiation of sprouting angiogenesis.

In addition to dissociation of mural cells from ECs, it is believed that transient disruption of the integrity of cell-to-cell binding is required to induce angiogenesis via transcellular extravasation into ischemic or inflammatory foci of proangiogenic hematopoietic cells as an accessory cell component.[9] EC-to-EC contact is regulated by different adhesion molecules, among which vascular endothelial (VE)-cadherin in particular plays essential roles in the formation of adherens junctions and in permeability control.[10] It was shown to be essential for the formation of stable blood vessels[11–13] and is also important for EC tube formation, inducing tube-like structures even when expressed in melanoma tumor cells.[14] Phosphorylation or endocytosis of VE-cadherin induced by activation of the VEGF receptor has been suggested to attenuate barrier function of ECs for leukocyte transmigration through the EC monolayer.[9] However, whether the transcription or translation of VE-cadherin is affected by VEGF has not been well established.

MicroRNAs (miRNAs or miRs) are endogenous short noncoding RNAs regulating gene expression either through translational inhibition or destabilization of target mRNA.[15] Crucial roles of miRNAs have been reported for many aspects of development, homeostasis and disease including tumor development.[16] Several lines of evidence suggest the involvement of miRNA in blood vessel formation.[17] Therefore, in the present study, we searched for miRNAs that are transiently endogenously upregulated in ECs on angiogenic switching and could inhibit angiogenesis if continuously overexpressed.

RESULTS

MiR-125b is upregulated in ECs under hypoxia or on stimulation with VEGF and inhibits their *in vitro* tube formation

We first analyzed the expression of miRs in ECs from hindlimb muscle subjected to hypoxia by the occlusion of the femoral artery. At 1 day after induction of ischemia, primary ECs ($CD31^+CD45^-$) from hindlimb muscles of mice were isolated by fluorescence-activated cell sorting. ECs from hindlimb muscle in the steady state acted as controls to compare the expression of miRs. Based on earlier reports of which miRs are expressed in ECs under different conditions,[17] we evaluated the expression of 20 miRs using

[1]Department of Signal Transduction, Research Institute for Microbial Diseases, Osaka University, Osaka, Japan and [2]JST, CREST, Tokyo, Japan. [3]These two authors contributed equally to this work. Correspondence: Professor N Takakura, Department of Signal Transduction, Research Institute for Microbial Diseases, Osaka University, 3-1 Yamada-oka, Suita, Osaka 565-0871, Japan. E-mail: ntakaku@biken.osaka-u.ac.jp
Received 7 March 2011; revised 27 January 2012; accepted 29 January 2012; published online 5 March 2012

quantitative reverse-transcription real-time PCR (qRT-PCR) analysis. Of these, we found that miRs 15b, 20b, 29a, 99a, 100, 103, 106b, 125b, 191 and 222 were increased by hypoxia (Figure 1a). We hypothesized that tumor cells may negatively regulate miRs that induce regression of blood vessels. Of the miRs overexpressed in ECs under tissue hypoxia, miRs 29a, 103 and 125b have been reported to be decreased in co-culture with tumor cells.[18] Here, we investigated the function of these miRs, as well as of miR-181a, which decreased in ECs either on hindlimb ischemia or co-culture with tumor cells, using *in vitro* tube formation of human umbilical vein ECs (HUVECs) as a readout. The results suggest that only miR-125b inhibits tube formation (Figure 1b). Therefore, we focused on miR-125b to study associations with angiogenesis.

Because miR-125b is upregulated in primary ECs under tissue hypoxia, we established the kinetics of its expression compared with miR-92a, which has been reported to be upregulated in ECs upon tissue hypoxia,[19] and snoRNA202, which is widely used as a nonregulated gene in various tissues. As shown in Figure 1c, miR-125b expression was transiently increased in ECs at 1 day after induction of ischemia and returned to basal level from day 2. miR-92a was also increased 1 day after induction of ischemia and gradually decreased thereafter.

Next, we assessed the expression of miR-125b in cultured HUVECs and tested whether this miR is upregulated upon angiogenic stimuli or hypoxia. First, we quantified the expression of miR-125b compared with miR-126, which is abundantly expressed specifically in ECs,[20] as well as with other miRs (Supplementary Figure S1). We found that miR125b is not highly expressed in HUVECs under the usual culture conditions. However, as with tissue hypoxia *in vivo*, we found that pro-angiogenic VEGF stimulation, as well as hypoxia (1.5% O_2), transiently induced miR-125b expression in cultured HUVECs (Figure 2a). VEGF is upregulated in ECs under tissue hypoxia. Therefore, hypoxia-mediated VEGF production in HUVECs may itself directly induce miR125b. However, hypoxia-induced miR125b is expressed earlier than VEGF in HUVECs, suggesting that other molecular cues associated with hypoxia induce miR125b. Moreover, basic fibroblast growth factor, a known pro-angiogenic factor, also induced miR-125b expression. Taken together, these data suggest the involvement of several growth factors for induction of miR-125b under conditions of tissue hypoxia similar to those that induce angiogenesis.

As recently reported, VEGF enhances the expression of p53,[21] and because several miRs are induced by p53 with the Drosha complex,[22,23] we tested whether miR125b expression is regulated by p53 in ECs. Small interfering RNA-mediated p53 knockdown inhibited VEGF-mediated induction of miR125b as well as constitutive expression of this miR (Figure 2b and Supplementary Figure S2).

a

ischemia/sham vascular EC miRNA expression change			
miRNA	**fold change↑**	**miRNA**	**fold change↓**
miR-15b	2.7	miR-16	0.07
miR-20b	91.9	miR-24	0.50
miR-29a	100.9	miR-31	0.09
miR-99a	12.6	miR-106a	0.14
miR-100	6.8	miR-125a	0.12
miR-103	30.3	miR-126-3p	0.40
miR-106b	9.02	miR-130a	0.11
miR-125b	2.03	miR-181a	0.20
miR-191	2.2	miR-221	0.36
miR-222	14.3	miR-320	0.14

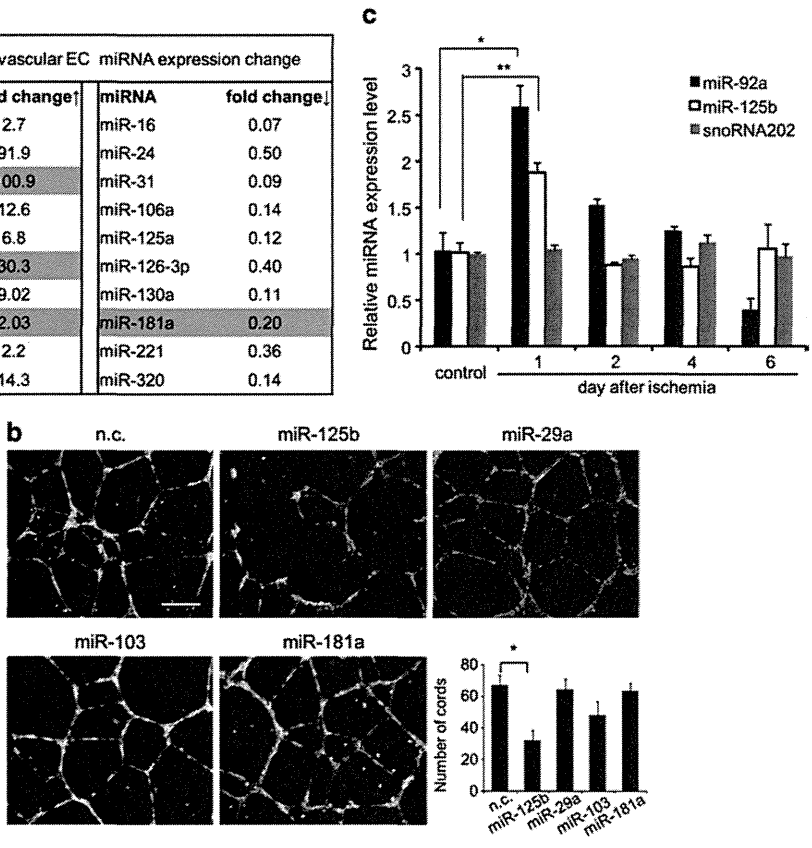

Figure 1. Screening of miRNAs upregulated on hypoxia and inhibiting EC tube formation. (**a**) List of significantly increased (fold change > 2.0) or decreased (fold change o 0.5) miRs in ECs affected by hindlimb ischemia. Mice were killed 24 h after induction of ischemia and $CD45^{-}CD31^{+}$ ECs from hindlimb muscle of three mice were sorted and pooled. The data are representative of one of three sets of experiments. Expression of each miR was normalized to RNU6, which is stably expressed under both tissue hypoxia and normoxia. (**b**) Screening for miRs inhibiting HUVEC tube formation. miRs including control miR (n.c.) as indicated were transfected into HUVECs. After 5 h, the cells were cultured for 20 h in Humedia EG2. They were then harvested, cultured for 10 h in 24-well plates coated with Matrigel and analyzed for tubule branching. For quantitative evaluation, we calculated the number of branches in six random fields. Bar indicates 200 μm. *Pb 0.05 (n = 3). (**c**) Time course of miR-125b expression analyzed by qRT-PCR in ECs from the hindlimb ischemia model. miR125b expression was compared with miR92a and snoRNA202 expression. snoRNA202 was used as a nonregulated gene in various tissues. ECs from three mice per experimental condition were pooled as in (**a**). Data show relative miR-125b or miR-92a expression, taking each miR in the steady state as unity. *Pb 0.01, **Pb 0.05 (n = 3).

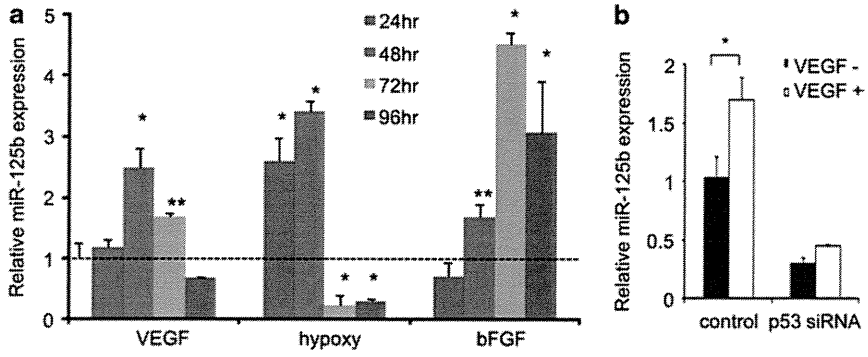

Figure 2. Induction of miR-125b expression in ECs by VEGF. (**a**) Induction of miR-125b expression in HUVECs. 2×10^5 HUVECs in six-well culture plates were serum starved for 6 h by culturing in Humedia EG2 without growth factors, and cultured in the presence or absence of VEGF (10 ng/ml) or basic fibroblast growth factor (bFGF; 5 ng/ml) or under hypoxic conditions (1.5% O_2) for the indicated times. miR-125b expression level by qRT-PCR was normalized to RNU6 using the comparative threshold cycle method. Level of miR-125b expression before stimulation with several factors was set as one. *P< 0.01, **P< 0.05 (n = 3). (**b**) miR-125b expression in HUVECs after p53 knockdown with RNA interference (RNAi). HUVECs were cultured in the presence or absence of VEGF for 24 h. *P< 0.05 (n = 3).

MiR-125b inhibits translation of VE-cadherin mRNA

It has been reported that miR-125b suppresses the expression of Her2 (human epidermal growth factor receptor-related 2) and Bak1 (BCL2-antagonist/killer 1),[24,25] but there are no reports on angiogenesis-related gene expression regulation by miR-125b. We employed several miR target prediction algorithms to identify putative miR-125b targets. We identified *VE-cadherin* as a target with a potential conserved binding site within its 3′ untranslated region (3′UTR) screened by TargetScan (Whitehead Institute for Biomedical Research, Cambridge, MA, USA); this sequence is evolutionarily conserved (Figure 3a). VE-cadherin is involved in tube formation by ECs by providing the adhesive component of endothelial adherens junctions.[2,9,10] Based on our results on tube formation in matrigel (Figure 1b), we hypothesized that miR-125b might downregulate synthesis of VE-cadherin by directly binding to sites within the 3′UTR of its message. To assess this possibility, we constructed luciferase reporter vectors encoding the complete wild-type 3′UTR of VE-cadherin mRNA as well as parallel control vectors containing mismatches in the predicted miR-125b binding site, or luciferase vectors containing no VE-cadherin UTR. As shown in Figure 3b, co-transfection of miR-125b with the luciferase reporter gene linked to the wild-type 3′UTR of human or mouse VE-cadherin resulted in a significant decrease in luciferase activity. In contrast, co-transfection of miR-125b with constructs containing mutated 3′UTR sequences did not result in decreased luciferase activity.

To confirm miR-125b-mediated modulation of endogenous VE-cadherin in ECs, HUVECs were transfected with miR-125b or control miR and expression of VE-cadherin on HUVECs assessed by western blotting and flow cytometry. An ~60% decrease of VE-cadherin expression resulted from the induction of miR-125b, using precursor molecules (pre-miR) (Figures 3c and d). We confirmed a reduction of cell surface VE-cadherin expression by flow cytometry (Figure 3e). We could not detect any alteration of VE-cadherin mRNA expression caused by miR-125b (Figure 3f). Indeed, inhibition of tube formation by miR-125b was abrogated by the overexpression of VE-cadherin (Figures 4a and b and Supplementary Figure S3); miR-125b inhibition did not enhance VE-cadherin expression (data not shown).

MiR-125b inhibits tumor growth mediated by severe hypoxia through disruption of EC tube formation

The results described above suggested that introduction of miR-125b into the tumor would inhibit angiogenesis and tumor growth. Before assessing the *in vivo* anti-angiogenic effect of injecting miR-125b into tumors, we tested its effects on tumor cells *in vitro*. Although it had been previously reported that miR-125b attenuated ErbB2 (erythroblastic leukemia viral oncogene homolog 2) expression and decreased proliferation of breast cancer cells *in vitro*,[24] our experiments failed to demonstrate any inhibitory effects of miR-125b on these parameters in Lewis lung carcinoma (LLC) or colon-26 cancer cells (Supplementary Figure S4).

We inoculated mice subcutaneously with tumor cells and started to inject miR-125b directly into the tumor using non-viral vectors composed of the cationic polymer polyethylenimine[26] when the tumor volume had reached 100 mm^3 (LLC: Figure 5) or 80 mm^3 (colon-26: supplementary Figure S5). Several weeks after injection of miR-125b, clear differences in the size of LLC and colon-26 tumors could be discerned (Figures 5a and b and Supplementary Figure S5a and b), but there were no differences between control and anti-miR-125-treated groups. In the group treated with anti-miR-125b, tumor growth might have been expected to increase compared with control because of the possibility of VE-cadherin expression enhancement. However, anti-miR-125b treatment did not markedly enhance VE-cadherin expression in the tumor environment. Moreover, we confirmed that enhancement of VE-cadherin expression was also not induced in HUVECs by anti-miR-125b transfection. Our study suggests that the level of miR-125b expression in tumor ECs is slightly upregulated (o 2.0-fold) but is not markedly higher than in ECs in normal skin, and that its localization therein is random, with no specific expression profile (data not shown). Therefore, anti-miR-125b may not enhance VE-cadherin expression in the tumor.

Real-time RT-PCR analysis confirmed significantly higher levels of miR-125b expression in tumors injected with miR-125b (Figure 5c and Supplementary Figure S5c). Essentially all $CD31^+$ ECs in control tumors expressed VE-cadherin, but in the miR-125b-transfected tumors, VE-cadherin expression by the majority of $CD31^+$ ECs was greatly reduced around the area of miR-125b injection (Supplementary Figure S6). Analysis of single-cell suspensions from each tumor confirmed the attenuation of endothelial VE-cadherin expression in miR-125b-injected tumors compared with controls (Figure 5d).

The miR-125b treatment significantly reduced the number of blood vessels in the tumor, but the difference was not marked (Figures 6a and b). On the other hand, morphological studies revealed indented irregular shaped blood vessels in miR-125b-injected tumors, not seen in controls. Moreover, we commonly found blood vessels stained with CD31 in miR-125b-treated tumors that were not stained by *in vivo* lectin perfusion, indicating lack of blood flow through them (Figure 6a). Assessing the state of

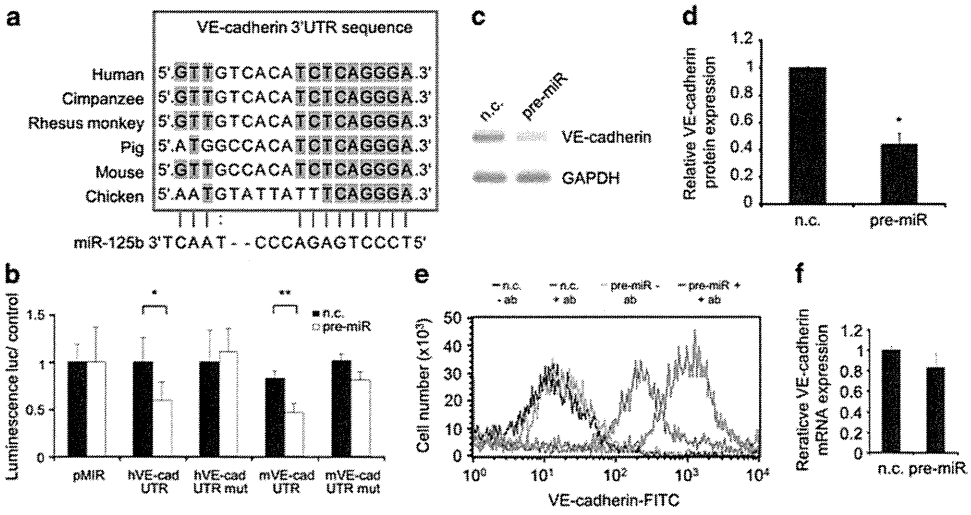

Figure 3. VE-cadherin is a direct target of miR-125b. (**a**) Alignment of potential miR-125b binding sites in the 3′UTR of the VE-cadherin mRNA of different species. (**b**) pMIR-REPORT vectors containing the 3′UTR of genes for wild-type human (h) or mouse (m) VE-cadherin (h or mVE-cad UTR) or mutated miR-125b binding site (h or mVE-cad UTR mut) and miR-125b (pre-miR) or control miR (n.c.) were co-transfected into HEK293 cells. The pMIR-REPORT vector containing no 3′UTR (pMIR) was used as a control set to unity. *P< 0.05, **P< 0.01 ($n=3$). (**c**) Western blot analysis of VE-cadherin expression in HUVECs transfected with control miR (n.c.) or miR-125b (pre-miR). Cell lysates were from HUVECs 48 h after transfection. GAPDH was used as an internal control. (**d**) Quantitative evaluation of VE-cadherin expression analyzed as described in (**c**). *P< 0.01 ($n=5$). (**e**) Cell surface expression of VE-cadherin in HUVECs treated as described in (**c**). Cells were stained with propidium iodide (PI) and fluorescein isothiocyanate (FITC)-conjugated anti-VE-cadherin antibody and analyzed by flow cytometry. PI-nonstained living cells were analyzed. −ab, cells stained by isotype-matched control IgG; +ab, cells stained with FITC-conjugated anti-VE-cadherin antibody. (**f**) qRT-PCR analysis of VE-cadherin expression in HUVECs transfected with control miR (n.c.) or miR-125b (pre-miR). mRNA was isolated 24 h after transfection of miR. The relative abundance of transcripts was normalized using the expression level of GAPDH mRNA. Error bar; there are no statistically significant differences ($n=3$).

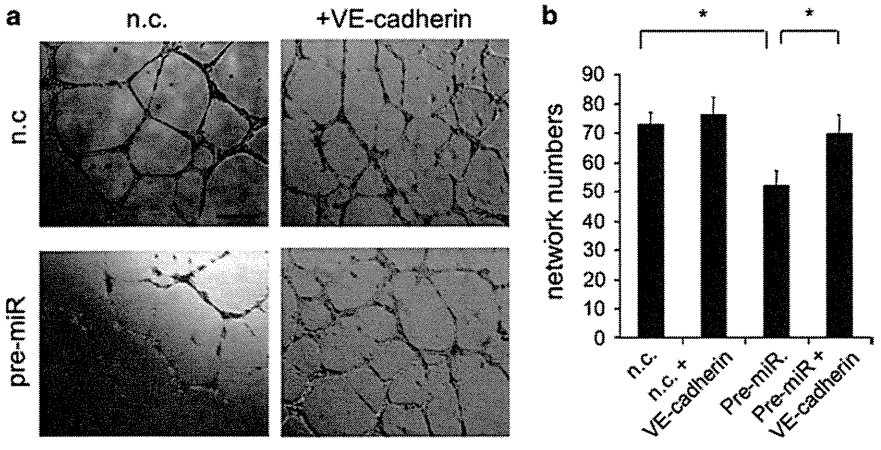

Figure 4. Rescue experiments. VE-cadherin overexpression in ECs transfected with miR-125b. (**a**) HUVECs transfected with control miR (n.c.) or miR-125b (pre-miR) with or without VE-cadherin expression vector assessed for tube formation. HUVECs were cultured for 20 h in Humedia EG2. Cells were then harvested and cultured for 10 h in 24-well plates coated with Matrigel. VE-cadherin almost completely rescued the miR-125b-induced decrease of tube formation. Bar indicates 200 μm. (**b**) For quantitative evaluation, we calculated the number of branches in six random fields. *P< 0.05.

hypoxia using hypoxyprobe showed that miR-125b-treated tumors were more hypoxic than controls (Figures 7a and b). Therefore, we concluded that miR-125b-suppressed VE-cadherin expression in ECs resulted in inhibition of tube formation, and because severe hypoxia is thus induced in the tumor environment, miR-125b inhibits tumor growth.

DISCUSSION

Here we report that miR-125b is upregulated in hypoxic ECs or on stimulation with VEGF or basic fibroblast growth factor. p53 is a regulator of miR-125b induction, but other mechanisms regulating its expression are also likely to exist. miR-125b binds directly to the 3′UTR of VE-cadherin mRNA and inhibits its translation. In contrast to upregulation of miR-125b expression, miR-125a was downregulated in ECs upon hypoxia. The seed sequences of miR-125a and miR-125b are identical, and downregulation of miR-125a may affect VE-cadherin expression; however, we focused on miR-125b, because we were seeking miRs that were upregulated and affected angiogenesis upon hypoxia.

When miR-125b is induced in ECs, their *in vitro* tube formation is suppressed by a mechanism involving inhibition of VE-cadherin

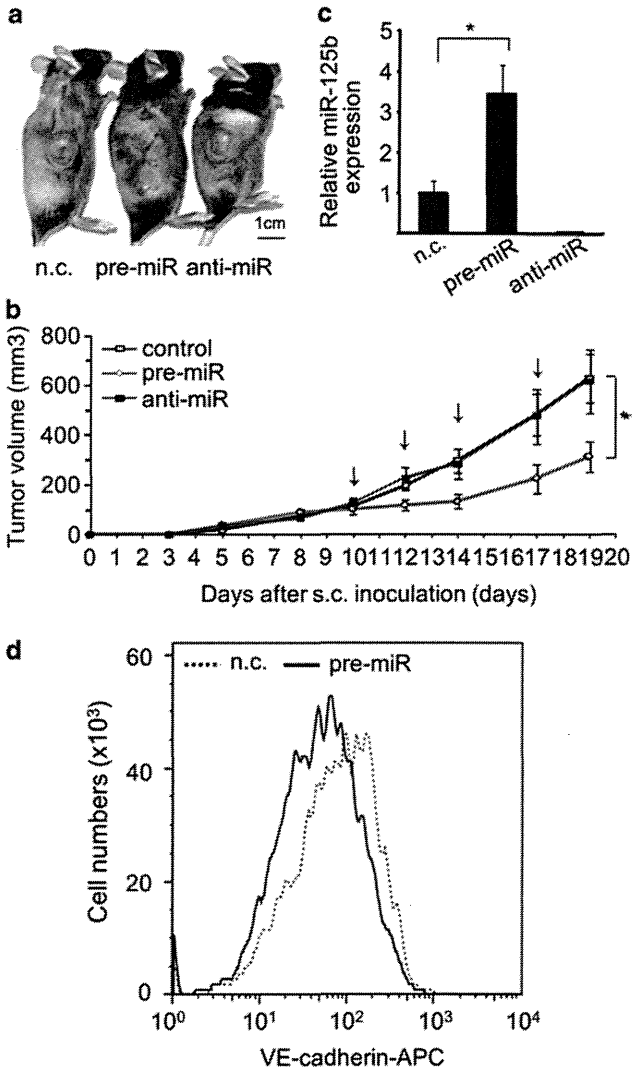

Figure 5. Suppression of tumor outgrowth by miR-125b. (**a**) Gross appearance of tumor-bearing mice 20 days after tumor cell inoculation. LLC cells (3×10^6) were inoculated subcutaneously into C57BL/6 mice. Anti-miR, anti-miR-125b; n.c., negative control; pre-miR, miR-125b. (**b**) Tumor growth suppressed by miR-125b but not by anti-miR-125b. Arrows indicate the day of miR injection. Tumor growth was monitored by calculating tumor volume on days 10, 12, 14, 17 and 19 after injection of miR-125 (pre-miR), anti-miR-125b (anti-miR) or negative control (control). *Pb 0.05 (n=3). (**c**) Detection of miR-125b expression in the tumor. At 2 days after injection of miR-125b, total RNA from tumor was isolated. A 3.5-fold increased level of miR-125b in the miR-125 (pre-miR)-injected group compared with the control miR (n.c.) group is seen. Anti-miR-125b suppressed the endogenous expression of miR-125b. Values normalized to RNU6 expression in each tumor were compared with the values obtained from the n.c. set at unity. *Pb 0.01 (n=3). (**d**) Suppression of VE-cadherin expression on ECs in the tumor. Single-cell suspensions from tumors injected with control miR (n.c.) or miR-125b (pre-miR) as described in (**a**) were stained with anti-VE-cadherin and anti-CD31 monoclonal antibodies (mAbs) and analyzed by flow cytometry. VE-cadherin expression on CD31-positive cells was analyzed. Mean intensity of VE-cadherin expression in these two groups was significantly different (Pb 0.05, n=5). The data shown are representative.

expression. This is confirmed by the finding that preceding overexpression of VE-cadherin in ECs prevents this suppression of tube formation by miR-125b. By blocking VE-cadherin expression in tumor ECs, miR-125b inhibited tumor outgrowth by disrupting EC tube formation. Although our studies have focused on ECs, we cannot completely exclude the possibility that miR-125b also affects other cell types in the tumor environment. However, as far as we could determine, miR-125b had no effect on tumor cell proliferation itself.

Induction of miR-125b expression in ECs of ischemic hindlimb muscle is transient, suggesting that miR-125b may have a role at the onset of angiogenesis in loosening EC contacts to allow extravasation of proangiogenic hematopoietic cells or bone marrow vascular progenitors into ischemic foci. We previously reported that many hematopoietic cells infiltrate into tumor sites from the edge of the tumor and that inhibition of migration of hematopoietic cells into the tumor inhibited tumor angiogenesis.[27] It is well known that hematopoietic cells can exert proangiogenic activity as an accessory cell component and that infiltration of these cells into the tumor environment occurs before ECs form blood vessels in the tumor.[27,28] Vascular endothelial cell-specific phosphotyrosine phosphatase (VE-PTP) is a phosphatase suppressing phosphorylation of VE-cadherin. Lack of VE-PTP leads to constitutive activation of VE-cadherin, resulting in suppression of normal angiogenesis.[29] Suppression of VE-cadherin function enhances the extravasation of hematopoietic cells.[30] Interestingly, pretreatment with anti-miR-125b in a tumor xenograft model led to retardation of tumor growth (Supplementary Figure S7). Moreover, preinduction of anti-miR-125b in HUVECs led to suppression of endothelial sprouting in a model using endothelial spheroids (Supplementary Figure S8). These findings suggest that transient downregulation of VE-cadherin expression is required for initiation of angiogenesis and that miR-125b may be involved in this process. However, further analysis is required to clarify the physiological function of miR-125b.

At the initiation of angiogenesis, it is widely accepted that Ang2, an antagonist of Ang1 that maintains stability of blood vessels by cell-to-cell adhesion between mural cells and ECs through the Tie2 receptor, is released from ECs to destabilize the vessels.[7,8] Hence, transient Ang2 expression is required for initiating angiogenesis, but its prolonged expression results in blood vessel regression under physiological or pathological conditions.[31] Thus far, no molecules other than Ang2 participating in transient destabilization of preexisting blood vessels have been identified. As tissue hypoxia or VEGF induces miR-125b expression in ECs, this miR may be involved in the initiation of angiogenesis by suppression of VE-cadherin expression. Although it is possible that the anti-angiogenic factor miR-125b is merely upregulated upon stimulation by pro-angiogenic factors as a negative feedback mechanism, but is not required for initiation of sprouting angiogenesis, our data suggest that excessively prolonged miR-125b expression prevents EC tube formation, leading to inhibition of tumor growth as observed in the Tie2/Ang2 system.

Our study suggests that ECs in the tumor environment express a little more miR-125b than other ECs. Nonetheless, the level of expression of miR125b was not particularly high, as described above. This is consistent with our initial hypothesis that tumor cells suppress expression of molecules in the tumor environment, which would mitigate against tumor growth. Indeed, when HUVECs were co-cultured with tumor cells, miR-125b expression was downregulated. Although this finding has already been reported by another group,[18] we found that VEGF co-stimulation in co-cultures of HUVECs and tumor cells resulted in slightly upregulated miR-125b expression in the former. However, the level of expression of this miR did not exceed the original level in HUVECs (Supplementary Figure S9). Therefore, tumor cell-derived factors must oppose VEGF effects for upregulation of miR-125b in ECs.

Molecular analysis of miRs has progressed rapidly and application of miRs in cancer therapy is being considered. One line of evidence showed involvement of miR-92a in vascular integrity by means of regulating the integrin subunit α-5, known to play an important role in angiogenesis.[19] It is suggested that

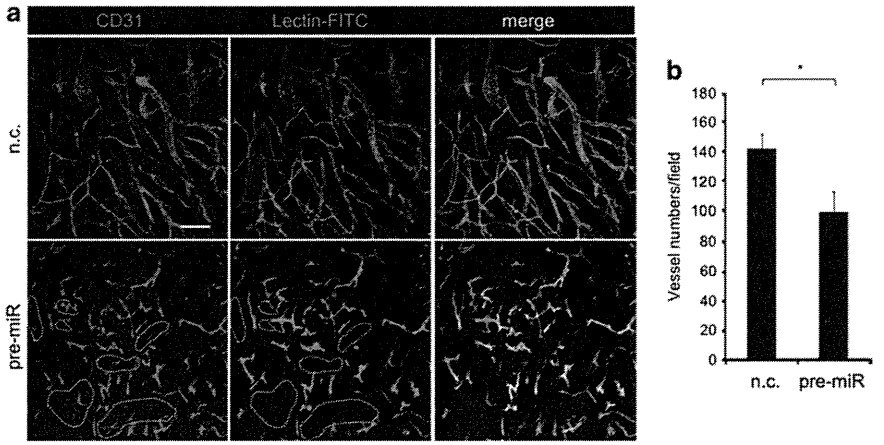

Figure 6. Disorganized structure of blood vessels induced by miR-125b. (**a**) ECs visualized with anti-CD31 antibody (red) and lectin staining (green) in the tumor. Treatment with miR-125b (pre-miR) induced disorganized vessel structure and blood vessels without blood flow (dashed area) suggesting nonfunctional blood vessels. n.c., negative control. Bar indicates 100 μm. (**b**) Quantitative evaluation of the number of lectin$^+$ blood vessels in n.c. or miR-125b-injected tumor, showing representative data for the number of blood vessels calculated in six random fields from one tumor of seven independent experiments. *P< 0.01.

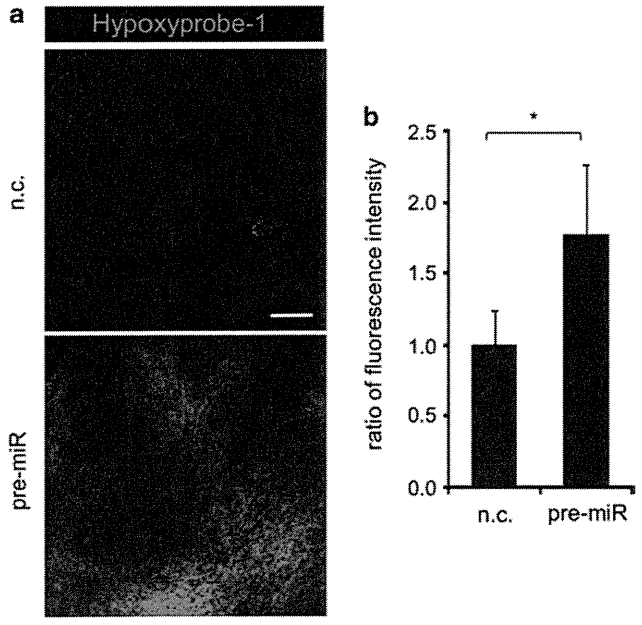

Figure 7. Hypoxia was induced by miR-125b injection. (**a**) Sections from tumors injected with control miR (n.c.) or miR-125b (pre-miR) were stained with anti-hypoxyprobe-1 (green). Hypoxyprobe-1 was injected into the peritoneal cavity before dissection. Bar indicates 50 μm. (**b**) Quantitative evaluation of the degree of hypoxia. The intensity of green fluorescence was measured using NIH image software (Bethesda, MD, USA) in 20 random fields. *P< 0.01.

overexpression of miR-92a inhibits angiogenesis by attenuating α-5 integrin expression in ischemic tissue. We found that miR92a is also transiently upregulated in ECs upon tissue hypoxia. Taken together with the results of the miR-125b study, it is suggested that miRNAs upregulated in ECs at the onset of angiogenesis may have an anti-angiogenic function; thus, it may be useful to identify anti-angiogenic miRs by this method. Using delivery of miRs directly into ECs in the tumor environment, miR-125b should be a good candidate for inhibition of tumor angiogenesis.

MATERIALS AND METHODS

Animals and cells

C57BL/6 mice were purchased from Japan SLC (Shizuoka, Japan). Animals were housed in environmentally controlled rooms of the animal experimentation facility at Osaka University. All experiments were carried out following the guidelines of Osaka University Committee for animal and recombinant DNA experiments. HUVECs (Kurabo, Osaka, Japan) were cultured in Humedia EG2. HUVECs were grown to confluence, serum starved and stimulated with VEGF (10 ng/ml; PeproTech, Rocky Hill, NJ, USA). Analyses such as of tube formation were performed as described.[32] LLC cells were maintained in Dulbecco's modified Eagle's medium (Sigma, St Louis, MO, USA) with 10% fetal bovine serum (Sigma) and penicillin/streptomycin (GIBCO, Rockville, MD, USA). A murine hindlimb ischemia model was established by the occlusion of the femoral artery as previously reported.[33] Sorting of primary ECs (CD31$^+$ CD45$^-$) from hindlimb muscle or tumor tissues was performed using a JSAN flow cytometer (Bay Bioscience, Kobe, Japan) as reported previously.[32] Tumor cell xenograft model was also as previously reported.[34] Preparation of single-cell suspensions from tumors and flow cytometric analysis were performed as previously described.[35]

Quantitative reverse-transcription real-time PCR

For miRs assessments, total RNA was extracted using PureLink miRNA Isolation Kits (Invitrogen, Carlsbad, CA, USA) and subjected to reverse transcription with the NCode miRNA First-Strand cDNA Synthesis and qRT-PCR Kits (Invitrogen) according to the manufacturer's instructions. qRT-PCR was performed with the Mx3000P QPCR System (Agilent Technologies Inc., Santa Clara, CA, USA) using Platinum SYBR Green qPCR SuperMix-UDG (Invitrogen). Results were normalized to RNU6 using the comparative threshold cycle method. Specific primers used in this experiment are described in Supplementary Table S1.

For detection of mRNA, total RNA was extracted using RNeasy mini kits (QIAGEN, Valencia, CA, USA) and reverse transcribed using the PrimeScript RT reagent Kit (Takara, Otsu, Japan) according to the manufacturer's instructions. qRT-PCR was performed as described above. Results were normalized to GAPDH (glyceraldehyde-3-phosphate dehydrogenase) with the comparative threshold cycle method. Specific primers used in this experiment were as follows: human VE-cadherin: 5′-ATCGGTTGTT CAATGCGTCC-3′ (sense) and 5′-CCTTCAGGATTTGGTACATGACA-3′ (anti-sense); human GAPDH: 5′-GAAGGTGAAGGTCGGAGTC-3′ (sense) and 5′-GAAGATGGTGATGGGATTTC-3′(anti-sense), and human p53: 5′-CTTCG AGATGTTCCGAGAGC-3′ (sense) and 5′-TTATGGCGGGAGGTAGACTG-3′ (anti-sense).

Transfection of plasmid, RNA interference and miRNA

For overexpression of miRs, 33 nM pre-miRs 125-b, 29a, 103 and 181a or pre-miR-control (Applied Biosystems, Foster City, CA, USA) were transfected into HUVECs using Lipofectamine 2000 (Invitrogen). After 5 h, the cells were cultured in Humedia EG2 until further analysis. For knockdown of p53, small interfering RNA (TP53 stealth select RNA interference; Invitrogen) or control small interfering RNA (Invitrogen) was introduced into HUVECs as described above. For the rescue experiment of VE-cadherin, the human VE-cadherin expression vector (a kind gift of Dr Fukuhara, NCVC, Osaka, Japan) was introduced into HUVECs with or without pre-miRs-125b, as described above.

In the tumor xenograft model, three million LLC cells were directly injected subcutaneously into the back flanks of 6-week-old female C57BL/6 mice. On days 10, 12, 14 and 17, we injected 400 pM control miR, pre-miR-125b or anti-miR-125b inhibitor (Applied Biosystems) using *in vivo*-jetPEI[26] (Polyplus Transfection, Illkirch, France) directly into the tumor mass. Measurements of tumor volume were performed as described previously.[35] Tumors were dissected for isolation of miRs and for immunofluorescence analysis 19 days after tumor cell inoculation.

Luciferase assays

The 3′UTR segments of human and mouse VE-Cadherin predicted to interact specifically with miR-125b were subcloned by standard procedures into the pMIR-REPORT Luciferase vector (Applied Biosystems) immediately downstream of the stop codon of the luciferase gene. In brief, we generated those oligos as follows: human VE-cadherin 3′UTR sense oligo (5′-CTAGTCCATGTGTCTTTACACCTCGCTGTTGTCACATCTCA GGGAACTGACCCTCAGGCACACCTGGATCCA-3′) ligated with the *Spe*1 site at the 3′ terminal and with *Bam*H1/*Hin*dIII at the 5′ terminal, and human VE-cadherin 3′UTR antisense oligo (5′-AGCTTGGATC CAGGTGTGCCTGAGGGTCAGTTCCCTGAGATGTGACAACAGCGAGGTGTAAA GACACATGGA-3′) ligated with the *Bam*H1/*Hin*dIII site at the 3′ terminal and with *Spe*1 at the 5′ terminal; human VE-cadherin 3′UTR mut (mutated sequences are underlined) sense oligo (5′-CTAGTCCATGTGTCTTTACA CCTCGCTGTTGTCACATCTTCAAACACTGACCCTCAGGCACACCTGGATCCA-3′) ligated with the *Spe*1 site at the 3′ terminal and with the *Bam*H1/*Hin*dIII at the 5′ terminal, and human VE-cadherin 3′UTR mut (mutated sequences underlined) antisense oligo (5′-AGCTTGGATCCAGGTGTGCCTGAGGGTCA GTGTTTGGAGATGTGACAACAGCGAGGTGTAAAGACACATGGA-3′) ligated with the *Bam*H1/*Hin*dIII site at the 3′ terminal and with the *Spe*1 at the 5′ terminal; mouse VE-cadherin 3′UTR sense oligo (5′-CTAGTCA CGCCACTCGCCTTTTGCCTAGTTGCCACATCTCAGGGAATGAACCTCACCCCCA GGGCGGATCCA-3′) ligated with the *Spe*1 site at the 3′ terminal and with the *Bam*H1/*Hin*d3 at the 5′ terminal, and mouse VE-cadherin 3′UTR antisense oligo (5′-AGCTTGGATCCGCCCTGGGGGTGAGGTTCATTCCCTGA GATGTGGCAACTAGGCAAAAGGCGAGTGGCGTGA-3′) ligated with the *Bam*H1/*Hin*dIII site at the 3′ terminal and with *Spe*1 at the 5′ terminal; mouse VE-cadherin 3′UTR mut (mutated sequences are underlined) sense oligo (5′-CTAGTCACGCCACTCGCCTTTTGCCTAGTTGCCACATCTTCAAACATG AACCTCACCCCCAGGGCGGATCCA-3′) ligated with the *Spe*1 site at the 3′ terminal and with the *Bam*H1/*Hin*dIII at the 5′ terminal, and mouse VE-cadherin 3′UTR mut (mutated sequences underlined) antisense oligo (5′-AGCTTGGATCCGCCCTGGGGGTGAGGTTCATGTTTGAAGATGTGGCAACT AGGCAAAAGGCGAGTGGCGTGA-3′) ligated with the *Bam*H1/*Hin*dIII site at the 3′ terminal and with *Spe*1 at the 5′ terminal. Double-stranded oligos were generated by annealing with sense and anti-sense oligos by standard methods and ligated into *Spe*1 and *Hin*dIII sites of the multiple cloning site of the pMIR-REPORT Luciferase vector. The vectors containing wild-type VE-cadherin or variant 3′UTR were transfected into HEK293 cells with or without miR-125b using Lipofectamine 2000. At 48 h after transfection, cells were lysed and luciferase activity was measured (POWERSCAN HT, DS Pharma Biomedical, Osaka, Japan). We used pMIR-REPORT β-gal control plasmid (Applied Biosystems) or pRL-TK plasmid (Promega, Madison, WI, USA) for normalization of luciferase values and the Dual-Glo Luciferase Assay System (Promega) for detection of luciferase activity.

Western blotting

Western blotting using anti-human VE-cadherin antibody was performed as previously described.[32] HUVECs were lysed 48 h after transfection with miR-125b or control miR.

Immunofluorescence

Tumor sections were stained with anti-mouse CD31 (Pharmingen, San Diego, CA, USA) and anti-mouse CD144 (VE-cadherin) antibody (BD Bioscience, San Diego, CA, USA). The procedure for tissue preparation and staining was as previously reported.[36] Lectin staining was performed as previously described[33] using fluorescein isothiocyanate-isolectin (Vector Lab, Burlingame, CA, USA). Hypoxic areas were identified by the fluorescein isothiocyanate-conjugated Hypoxyprobe-1 Mab1 (Natural Pharmacia International, Research Triangle Park, NC, USA). Samples were visualized using conventional microscopy (with a DM5500B equipped with HCX PL FLVOTAR 5/0.15 and HCX PL FLVOTAR 10/0.15 dry objective lenses; Leica, Solms, Germany) or confocal microscopy (Leica). Images were acquired with a DFC 500 digital camera (Leica) and processed with the Leica application suite (Leica) and Adobe Photoshop CS3 software (Adobe Systems, San Jose, CA, USA). All images shown are representative of 3–5 independent experiments.

Statistical analysis

All data were displayed as the mean s.d. and were analyzed by repeated-measures two-way analysis of variance or Student's *t*-test using Statview software (Abacus Concepts, Berkeley, CA, USA). A probability value of o 0.05 was considered statistically significant.

CONFLICT OF INTEREST

The authors declare no conflict of interest.

ACKNOWLEDGEMENTS

We thank S Fukuhara and N Mochizuki for supplying VE-cadherin expression plasmid, and K Fukuhara and N Fujimoto for technical assistance. This work was partly supported by a grant from the Ministry of Education, Science, Sports, and Culture of Japan.

REFERENCES

1 Risau W. Mechanisms of angiogenesis. *Nature* 1997; **386**: 671–674.
2 Dejana E. Endothelial adherens junctions: implications in the control of vascular permeability and angiogenesis. *J Clin Invest* 1996; **98**: 1949–1953.
3 Lindahl P, Johansson BR, Leveen P, Betsholtz C. Pericyte loss and microaneurysm formation in PDGF-B-deficient mice. *Science* 1997; **277**: 242–245.
4 Dumont DJ, Gradwohl G, Fong GH, Puri MC, Gertsenstein M, Auerbach A *et al.* Dominant-negative and targeted null mutations in the endothelial receptor tyrosine kinase, tek, reveal a critical role in vasculogenesis of the embryo. *Genes Dev* 1994; **8**: 1897–1909.
5 Sato TN, Tozawa Y, Deutsch U, Wolburg-Buchholz K, Fujiwara Y, Gendron-Maguire M *et al.* Distinct roles of the receptor tyrosine kinases Tie-1 and Tie-2 in blood vessel formation. *Nature* 1995; **376**: 70–74.
6 Suri C, Jones PF, Patan S, Bartunkova S, Maisonpierre PC, Davis S *et al.* Requisite role of angiopoietin-1, a ligand for the TIE2 receptor, during embryonic angiogenesis. *Cell* 1996; **87**: 1171–1180.
7 Augustin HG, Koh GY, Thurston G, Alitalo K. Control of vascular morphogenesis and homeostasis through the angiopoietin-Tie system. *Nat Rev Mol Cell Biol* 2009; **10**: 165–177.
8 Maisonpierre PC, Suri C, Jones PF, Bartunkova S, Wiegand SJ, Radziejewski C *et al.* Angiopoietin-2, a natural antagonist for Tie2 that disrupts in vivo angiogenesis. *Science* 1997; **277**: 55–60.
9 Vestweber D, Winderlich M, Cagna G, Nottebaum AF. Cell adhesion dynamics at endothelial junctions: VE-cadherin as a major player. *Trends Cell Biol* 2009; **19**: 8–15.
10 Dejana E, Tournier-Lasserve E, Weinstein BM. The control of vascular integrity by endothelial cell junctions: molecular basis and pathological implications. *Dev Cell* 2009; **16**: 209–221.

11 Gory-Faure S, Prandini MH, Pointu H, Roullot V, Pignot-Paintrand I, Vernet M *et al.* Role of vascular endothelial-cadherin in vascular morphogenesis. *Development* 1999; **126**: 2093-2102.
12 Carmeliet P, Lampugnani MG, Moons L, Breviario F, Compernolle V, Bono F *et al.* Targeted deficiency or cytosolic truncation of the VE-cadherin gene in mice impairs VEGF-mediated endothelial survival and angiogenesis. *Cell* 1999; **98**: 147-157.
13 Crosby CV, Fleming PA, Argraves WS, Corada M, Zanetta L, Dejana E *et al.* VE-cadherin is not required for the formation of nascent blood vessels but acts to prevent their disassembly. *Blood* 2005; **105**: 2771-2776.
14 Hendrix MJ, Seftor EA, Meltzer PS, Gardner LM, Hess AR, Kirschmann DA *et al.* Expression and functional significance of VE-cadherin in aggressive human melanoma cells: role in vasculogenic mimicry. *Proc Natl Acad Sci USA* 2001; **98**: 8018-8023.
15 Bartel DP. MicroRNAs: genomics, biogenesis, mechanism, and function. *Cell* 2004; **116**: 281-297.
16 Krek A, Grun D, Poy MN, Wolf R, Rosenberg L, Epstein EJ *et al.* Combinatorial microRNA target predictions. *Nat Genet* 2005; **37**: 495-500.
17 Suarez Y, Sessa WC. MicroRNAs as novel regulators of angiogenesis. *Circ Res* 2009; **104**: 442-454.
18 Wurdinger T, Tannous BA, Saydam O, Skog J, Grau S, Soutschek J *et al.* miR-296 regulates growth factor receptor overexpression in angiogenic endothelial cells. *Cancer Cell* 2008; **14**: 382-393.
19 Bonauer A, Carmona G, Iwasaki M, Mione M, Koyanagi M, Fischer A *et al.* MicroRNA-92a controls angiogenesis and functional recovery of ischemic tissues in mice. *Science* 2009; **324**: 1710-1713.
20 Kuehbacher A, Urbich C, Zeiher AM, Dimmeler S. Role of Dicer and Drosha for endothelial microRNA expression and angiogenesis. *Circ Res* 2007; **101**: 59-68.
21 Chen YH, Wu HL, Chen CK, Huang YH, Yang BC, Wu LW. Angiostatin antagonizes the action of VEGF-A in human endothelial cells via two distinct pathways. *Biochem Biophys Res Commun* 2003; **310**: 804-810.
22 Yamakuchi M, Lotterman CD, Bao C, Hruban RH, Karim B, Mendell JT *et al.* P53-induced microRNA-107 inhibits HIF-1 and tumor angiogenesis. *Proc Natl Acad Sci USA* 2010; **107**: 6334-6339.
23 Suzuki HI, Yamagata K, Sugimoto K, Iwamoto T, Kato S, Miyazono K. Modulation of microRNA processing by p53. *Nature* 2009; **460**: 529-533.
24 Scott GK, Goga A, Bhaumik D, Berger CE, Sullivan CS, Benz CC. Coordinate suppression of ERBB2 and ERBB3 by enforced expression of micro-RNA miR-125a or miR-125b. *J Biol Chem* 2007; **282**: 1479-1486.
25 Shi XB, Xue L, Yang J, Ma AH, Zhao J, Xu M *et al.* An androgen-regulated miRNA suppresses Bak1 expression and induces androgen-independent growth of prostate cancer cells. *Proc Natl Acad Sci USA* 2007; **104**: 19983-19988.
26 Niola F, Evangelisti C, Campagnolo L, Massalini S, Bue MC, Mangiola A *et al.* A plasmid-encoded VEGF siRNA reduces glioblastoma angiogenesis and its combination with interleukin-4 blocks tumor growth in a xenograft mouse model. *Cancer Biol Ther* 2006; **5**: 174-179.
27 Okamoto R, Ueno M, Yamada Y, Takahashi N, Sano H, Suda T *et al.* Hematopoietic cells regulate the angiogenic switch during tumorigenesis. *Blood* 2005; **105**: 2757-2763.
28 Takakura N. Role of hematopoietic lineage cells as accessory components in blood vessel formation. *Cancer Sci* 2006; **97**: 568-574.
29 Baumer S, Keller L, Holtmann A, Funke R, August B, Gamp A *et al.* Vascular endothelial cell-specific phosphotyrosine phosphatase (VE-PTP) activity is required for blood vessel development. *Blood* 2006; **107**: 4754-4762.
30 Gotsch U, Borges E, Bosse R, Boggemeyer E, Simon M, Mossmann H *et al.* VE-cadherin antibody accelerates neutrophil recruitment in vivo. *J Cell Sci* 1997; **110** (Pt 5): 583-588.
31 Holash J, Maisonpierre PC, Compton D, Boland P, Alexander CR, Zagzag D *et al.* Vessel cooption, regression, and growth in tumors mediated by angiopoietins and VEGF. *Science* 1999; **284**: 1994-1998.
32 Kidoya H, Ueno M, Yamada Y, Mochizuki N, Nakata M, Yano T *et al.* Spatial and temporal role of the apelin/APJ system in the caliber size regulation of blood vessels during angiogenesis. *EMBO J* 2008; **27**: 522-534.
33 Yamada Y, Takakura N. Physiological pathway of differentiation of hematopoietic stem cell population into mural cells. *J Exp Med* 2006; **203**: 1055-1965.
34 Kidoya H, Kunii N, Naito H, Muramatsu F, Okamoto Y, Nakayama T *et al.* The apelin/APJ system induces maturation of the tumor vasculature and improves the efficiency of immune therapy. *Oncogene* 2012; **31**: 3254-3264.
35 Nagahama Y, Ueno M, Miyamoto S, Morii E, Minami T, Mochizuki N *et al.* PSF1, a DNA replication factor expressed widely in stem and progenitor cells, drives tumorigenic and metastatic properties. *Cancer Res* 2010; **70**: 1215-1224.
36 Takakura N, Watanabe T, Suenobu S, Yamada Y, Noda T, Ito Y *et al.* A role for hematopoietic stem cells in promoting angiogenesis. *Cell* 2000; **102**: 199-209.

Supplementary Information accompanies the paper on the Oncogene website (http://www.nature.com/onc)